Morphology and Thermodynamics of Symmetric Poly(A-*block*-B-*block*-C) Triblock Copolymers

Reimund Stadler,*,† Clemens Auschra,†,‡ Jörg Beckmann,†,§ Udo Krappe,† Ingrid Voigt-Martin,‖ and Ludwik Leibler⊥

Institut für Organische Chemie, Johannes Gutenberg Universität Mainz, J. J. Becher Weg 18-20, D-55099 Mainz, Germany, Institut für Physikalische Chemie, Johannes Gutenberg Universität Mainz, J. Welderweg 12, D-55099 Mainz, Germany, and Ecole Superieur de Physique et Chimie Industrielle (ESPCI), 10 Rue Vauquelin, 75231 Paris Cedex 05, France

Received August 23, 1994; Revised Manuscript Received December 12, 1994®

ABSTRACT: The morphology of ABC triblock copolymers based on polystyrene-*block*-polybutadiene-*block*-poly(methyl methacrylate) [PS-*b*-PB-*b*-PMMA] (SBM series) and their hydrogenated analogues polystyrene-*block*-poly(ethylene-*co*-butylene)-*block*-poly(methyl methacrylate) [PS-*b*-PEB-*b*-PMMA] (SEBM series) block copolymers is governed by the relatively weak incompatibility of the end blocks PS and PMMA in comparison to the strong incompatibility of the polybutadiene or poly(ethylene-*co*-butylene) midblock. The paper describes the morphologies of high molecular weight ($M_n \approx 200\,000$) block copolymers, which are symmetrical with respect to the PS and the PMMA blocks with a varying elastomeric center block ($0.06 < w_{el} < 0.38$). Besides an ABC lamellar morphology (ll) (38 wt % PB or PEB), two other lamellar morphologies are observed for shorter elastomer chains: At 17 wt % of the elastomeric center block a "cylinder at the wall" morphology is observed where PB or PEB cylinders are located at the lamellar PS/PMMA interface (lc). At 6 wt % of elastomer, the polybutadiene forms spheres at the PS/PMMA interface ("ball at the wall") (ls). In this case hydrogenation of the butadiene block, which is associated with a further increase in the immiscibility to the end blocks, induces a change of the overall lamellar structure into a cylindrical morphology in which PS cylinders surrounded by PEB rings are dispersed in a PMMA matrix (cr). The transition from the lamellar (ll) morphology to the (lc) and (ls) morphologies is described by a simple extension of the Meier/Alexander/de Gennes/Semenov theories of AB block copolymers in the strong segration limit to ABC block copolymers. The theoretical description predicts that morphological transitions can be achieved in ABC triblock copolymers at constant composition even in the limit of strong segregation.

Introduction

The detailed analysis of ordered spherical, cylindrical, and lamellar morphologies in AB and ABA block copolymers as well as $(AB)_n$ starblock copolymers dates back to the seventies and early eighties.[1−3] In 1986 the bicontinuous double-diamond morphology was recognized.[4,5] The theoretical framework to calculate the free energy of phase-segregated block copolymers in the "strong segregation limit" has become available through the work of Meier[6] and Helfand.[7−9] Alexander[10] and de Gennes[11] gave a simple description of polymer brushes attached to surfaces which has been extended by Semenov[12] to the description of spherical, cylindrical, and lamellar morphologies. There has recently been some doubt in the stability of bicontinuous double-diamond morphologies, both experimentally[13] and theoretically.[14] Instead, a gyroid phase has been reported by Hajduk et al.[15] which is a stable structure according to Schick et al.[16] More recently, the order−disorder transition in block copolymers[17−20] in the "weak segregation limit" as first predicted by Leibler[21] and extended by Frederickson and Helfand[22] and the organization of block copolymers at interfaces (polymer/air or polymer/polymer interfaces) has been studied in detail both theoretically[23−26] and experimentally.[27−30] A recent review has been given by Binder.[31] More complex chain topologies like the linear $(AB)_n$ blocks[32] have been synthesized recently and discussed with respect to their potential to control the morphology. Other recent work in two-component block copolymers is related to the grain structure[33] in such systems and to the morphological changes induced in mixtures of multiblock copolymers.[34]

In contrast to block copolymers consisting of two chemically different blocks only a limited amount of information is available for ABC triblock copolymers consisting of three chemically different species. Riess et al. proposed a general scheme of possible types of morphologies;[35] however—due to the limited amount of experimental data in this work—many questions remain in the area of ABC triblock copolymers. In the Riess scheme the volume fraction of the components was the main parameter determining the morphology. Most of the proposed morphologies show core−shell type structures. Extensive work on block copolymers based on styrene, butadiene, and vinylpyridine by Kotaka et al.[36,37] and styrene, [(*N*,*N*-dimethylamino)methyl]-styrene, and isoprene[38,39] resulted in the first more detailed picture of ABC triblock copolymer morphologies. Hashimoto et al. gave a first description based on an extension of the Helfand model.[7−9] Recently, new ordered morphologies have been recognized in ABC triblock systems. Mogi et al.[40,41] showed the existence of a highly ordered tricontinuous double-diamond morphology in a PI-*b*-PS-*b*-PVP triblock copolymer, as well as a morphology in which the PI and the PVP domains form cylinders in a PS matrix. The same group discussed the molecular weight dependence of lamellar PI-*b*-PS-*b*-PVP block copolymers.[42] As in the case of diblock copolymers, the lamellar long period scales with $M^{2/3}$. The lamellar morphology formed at a composition which contains about equal amounts of the three

* To whom all correspondence should be addressed.
† Institut für Organische Chemie.
‡ Present address: Röhm GmbH, Darmstadt, FRG.
§ Present address: NIST, Gaithersburg, MD.
‖ Institut für Physikalische Chemie.
⊥ Ecole Superieur de Physique et Chimie Industrielle.
® Abstract published in *Advance ACS Abstracts,* March 15, 1995.

0024-9297/95/2228-3080$09.00/0

Table 1. Characteristics of Triblock Copolymers

copolymer	$10^{-3} M_n$[a]	M_w/M_n[c]	w_{PS}	ϕ_{PS}	$w_{PB/PEB}$	$\phi_{PB/PEB}$	w_{PMMA}	ϕ_{PMMA}
			PS-*block*-PB-*block*-PMMA					
SBM6	225	1.11	0.45	0.47	0.06	0.075	0.49	0.455
SBM17	238	1.10	0.48	0.48	0.17	0.20	0.35	0.32
SBM38	245	1.08	0.24	0.23	0.38	0.44	0.38	0.33
			PS-*block*-PEB-*block*-PMMA					
SEBM6	226[b]	1.12	0.45	0.47	0.06	0.075	0.49	0.455
SEBM17	240[b]	1.13	0.48	0.48	0.17	0.20	0.35	0.032
SEBM38	248[b]	1.15	0.23	0.23	0.39	0.45	0.37	0.32

[a] Determined by membrane osmometry (toluene, 25 °C). [b] Calculated on the basis of the PB weight fraction of the SBM series. [c] GPC calibrated with PS.

constituents. Using the same components and the same composition but a different block sequence (PS-*b*-PI-*b*-PVP), Thomas et al. showed the existence of a cylindrical core–shell morphology with nonuniform mean curvature of the interface.[43] At first sight the switching of the morphology from ABC lamellar to a core–shell morphology is rather surprising. However, as will be discussed below, this can be easily explained on the basis of the relative imcompatibilities of the three components.

In a recent paper we presented first morphological studies on polystyrene–*block*-poly(ethylene-*co*-butylene)-*block*-poly(methyl methacrylate) (PS-*b*-PEB-*b*-PMMA) triblock copolymers[44] and gave some qualitative arguments how the morphology is controlled by the relative incompatibilities. The block copolymers have molecular weights around 200 000. They are symmetric with respect to the PS and PMMA end blocks. The fractions of PEB center block were 38, 17, and 6 wt %, respectively. While a lamellar morphology is expected in the absence of the hydrogenated polybutadiene blocks, electron microscopy has shown that these triblocks exhibited new, hitherto unseen, morphologies. The block copolymer with 39 wt % of PEB shows a lamellar morphology, while a lamellar morphology with regular PEB cylinders located at the interface of PS and PMMA lamellae is formed at a PEB level of 17 wt %. Even more surprising was the result that the triblock system with a PEB content of only 6 wt % shows PS cylinders dispersed in the PMMA matrix (see below). In contrast to this result, the corresponding block copolymer with nonhydrogenated polybutadiene block shows a lamellar PS/PMMA morphology with polybutadiene spheres located at the lamellar interface ("ball at the wall" morphology).[45] These experimental findings have been explained qualitatively on the basis of differences in the relative incompatibility between the three polymeric components. The interfacial tension between PEB/PMMA and PEB/PS is much larger than between the "less" immiscible PS/PMMA pair. It has been argued that the observed morphologies result from the minimization of the unfavorable A/B and B/C contacts. As a consequence of this behavior such ABC block copolymers exhibit new morphologies not only as bulk materials but also as compatibilizers in blends of components miscible with A and C.[46] The variation of the morphology upon hydrogenation may result not only from the variation of the interaction parameter but also from the variation of the Kuhn segment length and segmental volume. Changing the Kuhn length may lead to a spontaneous curvature. As has been discussed by Adjari and Leibler,[47] the asymmetry of the Kuhn length and segmental volume induces repulsions and governs the interaction parameter in polyolefins.

In the present contribution the morphologies of the PS-*b*-PEB-*b*-PMMA triblock copolymers will be analyzed in some more detail and compared to the morphologies of the corresponding nonhydrogenated PS-*b*-PB-*b*-PMMA block copolymers. The free energy of these triblock systems is calculated on the basis of a simple extension of the Alexander/deGennes and Semenov description of polymer brushes and microphase-separated systems. It will be shown that the experimentally observed morphologies can be adequately described by simple theoretical arguments. For ABC block copolymers with lamellar morphology an extension of the Helfand theory has been recently reported by Mogi et al.[42] An alternative theoretical description has been given by Ohta et al.[48] These authors succeeded in the description of ABC lamellar structures as well as morphologies where both A and C spheres and cylinders are dispersed in the B matrix and attempted a first theoretical analysis of the ordered tricontinuous double-diamond structure observed by Mogi et al.[41] Spontak et al.[49] reported a more elaborate extension of the Semenov theory to lamellar ABC triblock copolymers. Birshtein and Lyatskova recently described theoretically the morphology variation observed upon variation of the block sequence (Mogi et al.,[40] Gido et al[43]) using a similar approach based on a theory of polymer brushes.[50]

Experimental Section

Synthesis of polystyrene-*block*-polybutadiene-*block*-poly(methyl methacrylate) (SBM series) and polystyrene-*block*-poly(ethylene-*co*-butylene)-*block*-poly(methyl methacrylate) (SEBM series) block copolymers was accomplished by sequential anionic polymerization of styrene, butadiene, and methyl methacrylate in tetrahydrofuran (thf) in the presence of lithium alkoxides using *sec*-butyllithium as initiator.[51] The butadiene block of the copolymer which consisted predominantly of 1,2-structural units was subsequently hydrogenated via diimine reduction in the SEBM series. Details of the synthetic procedures, including the detailed characterization of the PS and PS-*b*-PB precursor polymers are given elsewhere.[51] A study of the thermal stability of the hydrogenated system is given in ref 52. Table 1 summarizes the characteristics of the triblock copolymers used in this study.

Sample Preparation. Transparent bluish films of the pure triblock copolymers were slowly cast from $CHCl_3$ (SBM series and SEBM series) and toluene (SBM series). For further equilibration the dry films were annealed at 160 °C for 5 days (SEBM series). To avoid cross-linking of the nonhydrogenated 1,2-polybutadiene block, the drying and annealing of the SBM series was performed at 85 °C for 2 days, followed by a thermal treatment at 150 °C under high vacuum for 2, 4, and 6 h. No change in the morphology was observed for the different annealing conditions.

Transmission electron microscopy (TEM) was performed on a Philips transmission electron microscope

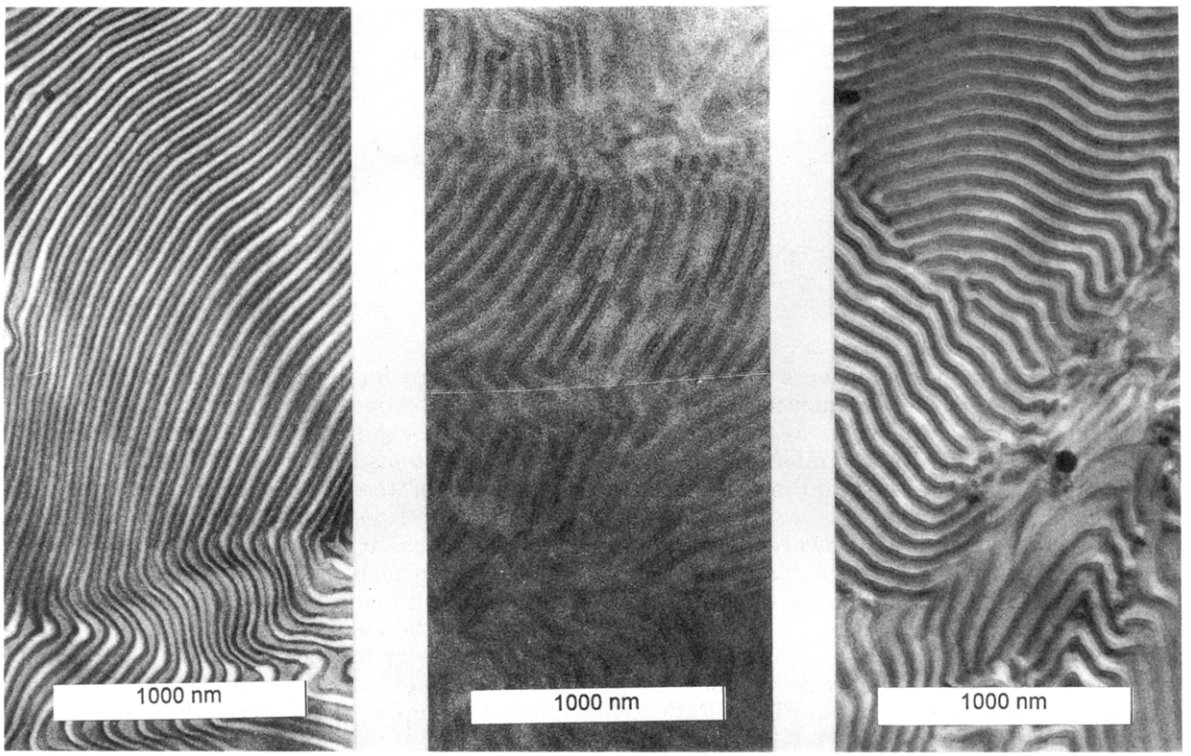

Figure 1. Transmission electron micrographs of polystyrene-*block*-polybutadiene-*block*-poly(methyl methacrylate) (SBM38) and polystyrene-*block*-poly(ethylene-*co*-butylene)-*block*-poly(methyl methacrylate) (SEBM38): (a, left) SBM38, stained with OsO_4; (b, middle) SBM38, stained with RuO_4; (c, right) SEBM 38, stained with RuO_4.

operating at 80 kV. Ultrathin sections of the block copolymers were obtained using a Reichert ultramicrotome equipped with a diamond knife. The rigidity of the SEBM series and sample SBM6 was high enough to prepare high-quality ultrathin sections at room temperature. Ultrathin sections of SBM17 and SBM38 were obtained by cryo-ultramicrotoming. The ultrathin sections were stained using the ruthenium tetraoxide or osmium tetroxide.

Results and Discussion

A. Electron Microscopy. A preliminary discussion of the morphologies realized in symmetric PS-*b*-PEB-*b*-PMMA triblock copolymers of variable PEB block length has been given in our previous paper of this series.[44] In the present section the electron microscopic results of the SEBM series will be compared to the corresponding nonhydrogenated analogues (SBM series).

Parts a–c of Figure 1 show electron micrographs of SEBM38 (RuO_4 stained) and SBM38 (RuO_4 stained and OsO_4 stained). As expected, a lamellar morphology is formed in these polymers where the components are present in about equal amounts. We will denote this morphology as (ll) throughout this paper. In the RuO_4-stained samples the PS lamellae (in SEBM38) and the PS and the PB lamellae (in SBM38) appear dark, because both the PS and the PB are readily attacked by this staining agent. PMMA does not react with RuO_4 under the applied staining conditions and therefore appears bright. In SEBM38 the intermediate EB lamellae are weakly stained and appear light gray. The long period the lamellar structure formed by an ABC block copolymer is [...ABCB...]. From the micrographs of SEBM 38 (i.e. Figure 1c) the long period involving ~PS~PEB~PMMA~PEB~ as determined from the micrograph is 90–95 nm. From the volume fractions of the components, the contributions of the individual components to the long period can be calculated. The data are summarized in Table 2.

Table 2. Dimensions of Block Copolymer Microphases Obtained from Transmission Electron Microscopy[a]

L_{ll}, nm	L_{PS}, nm	$L_{PB/PEB}$, nm	L_{PMMA}, nm
		SBM38	
62 ± 6	12.5 ± 0.5	2 × 14.5 ± 0.4	20 ± 4
		SEBM38	
≈90–95	≈23	2 × ≈18	≈35

L_{lc}, nm	D_{cyl}, nm	$D_{PB/PEB}$, nm	L_{PS}, nm	L_{PMMA}, nm
		SBM17		
44 ± 1	30.3 ± 0.5	13.1 ± 0.2	26.4 ± 0.7	17.7 ± 0.6
		SEBM17		
≈65–70	≈25–30	≈10–15	≈35–40	≈30–35

L_{ls}, nm	D_{sph}, nm	D_{PB}, nm	L_{PS}, nm	L_{PMMA}, nm
		SBM6		
52.6 ± 0.5	18	9.0 ± 2	28.1 ± 0.6	24.5 ± 5

L_{cr}, nm	D_{ring}, nm	D_{PEB}, nm	D_{PS}, nm
		SEBM6	
≈55–65	≈20–25	≈5–10	≈30–35

[a] (ll): L_{ll} = lamellar long period of (ll) morphology; $L_{PS,PMMA,PB,PEB}$ = thickness of corresponding lamella. (lc): L_{lc} = lamellar long period of (lc) morphology; D_{cyl} = periodicity between cylinders; D_{PEB} = diameter of PEB cylinders. (ls): L_{ls} = lamellar long period of (ls) morphology; D_{sph} = periodicity between spheres; D_{PB} = diameter of the PB sphere; $L_{PS,PMMA}$ = thickness of corresponding lamella. (cr): L_{cr} = cylinder long period of (cr) morphology; D_{ring} = periodicity between PEB rings; D_{PEB} = diameter of PEB rings; D_{PS} = diameter of the PS cylinder.

In the OsO_4-stained sample of the corresponding SBM38 polymer (Figure 1a) two polybutadiene lamellae are formed per morphological repeating unit. In the RuO_4-stained sample both the PS and the PB segments are attacked (Figure 1b). The long period of SBM38 is ≈62 nm. This is considerably smaller than the long period of the hydrogenated block copolymer.

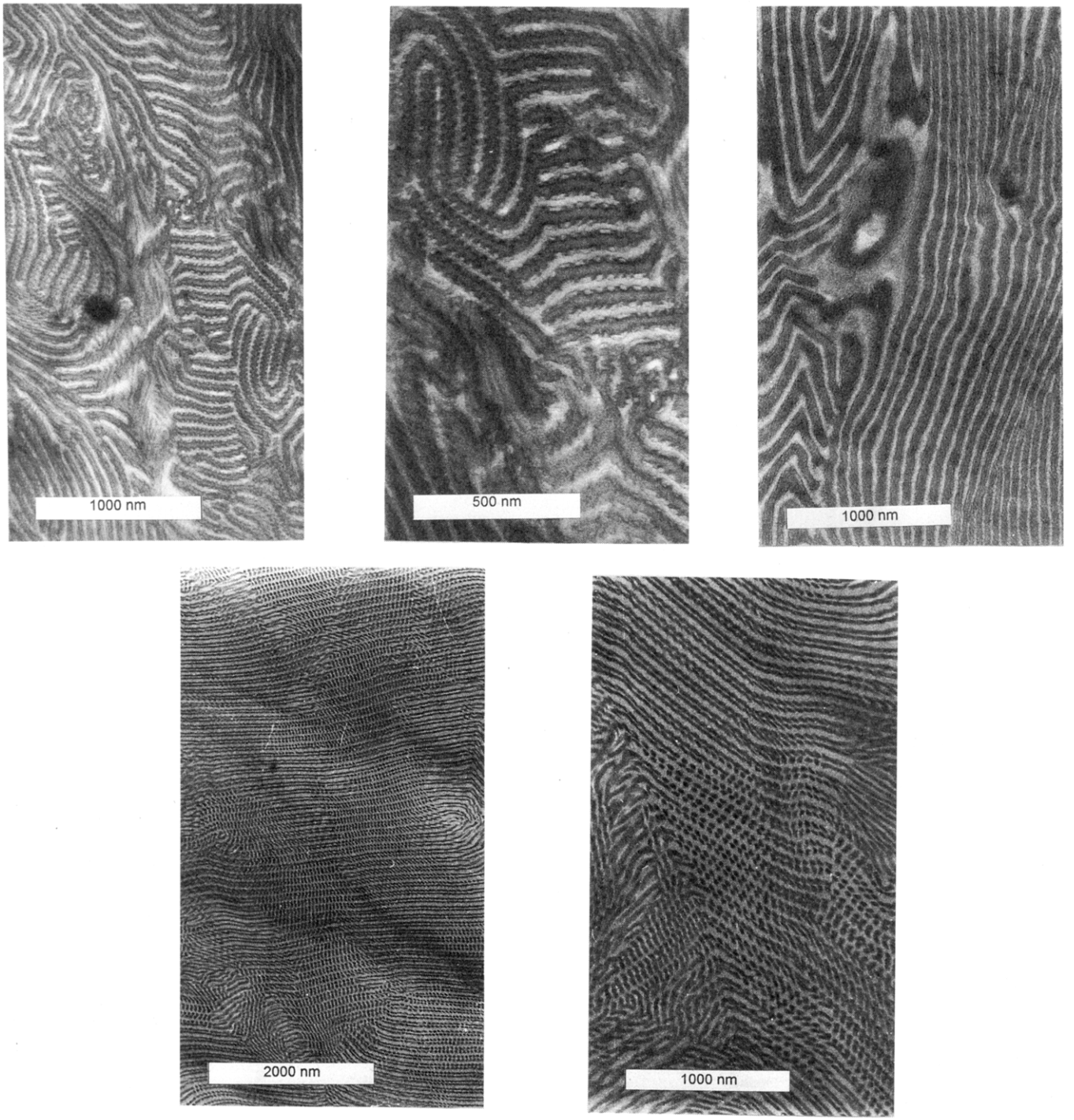

Figure 2. Transmission electron micrographs of polystyrene-*block*-polybutadiene-*block*-poly(methyl methacrylate) (SBM17) and polystyrene-*block*-poly(ethylene-*co*-butylene)-*block*-poly(methyl methacrylate) (SEBM17): (a, b; top left and middle) SEBM17, stained with RuO_4; (c, top right) SBM17, stained with RuO_4; (d, e; bottom left and right) SBM 17, stained with OsO_4.

The long periods have been obtained by averaging over large sets of lamellae, considering the effect of partial imperfect orientation (tilting) of the lamellar stacks.

Parts a–e of Figure 2 show electron micrographs of SEBM17 and SBM17. In both polymers the gross morphology is still lamellar.

In the case of SEBM 17 the lamellar surfaces are not flat anymore but have a very regular modulation.[44] From the micrograph at the higher magnification (Figure 2b) the structure can be elucidated unambiguously. The surface modulation is the result of the formation of cylinders of the EB block at the PMMA/PS phase boundary. Figure 3a gives a schematic representation of this structure. This morphology will be assigned as (lc) in the following. Due to the staining conditions no contrast is developed between the PEB microdomains and the PMMA lamellae, but the PEB/PMMA boundary is stained to a larger extent, allowing the recognition of the PEB cylinders. The assignment of a cylindrical morphology to the PEB phase is based on the following arguments: In the case of PEB ellipses or spheres the cross section of the PEB phase would appear less regular. Because the ultrathin section is not always perpendicular to the cylinder direction, the PEB cylinder cross sections appear as regular ellipses (Figure 3b). In some sections of the micrograph regions

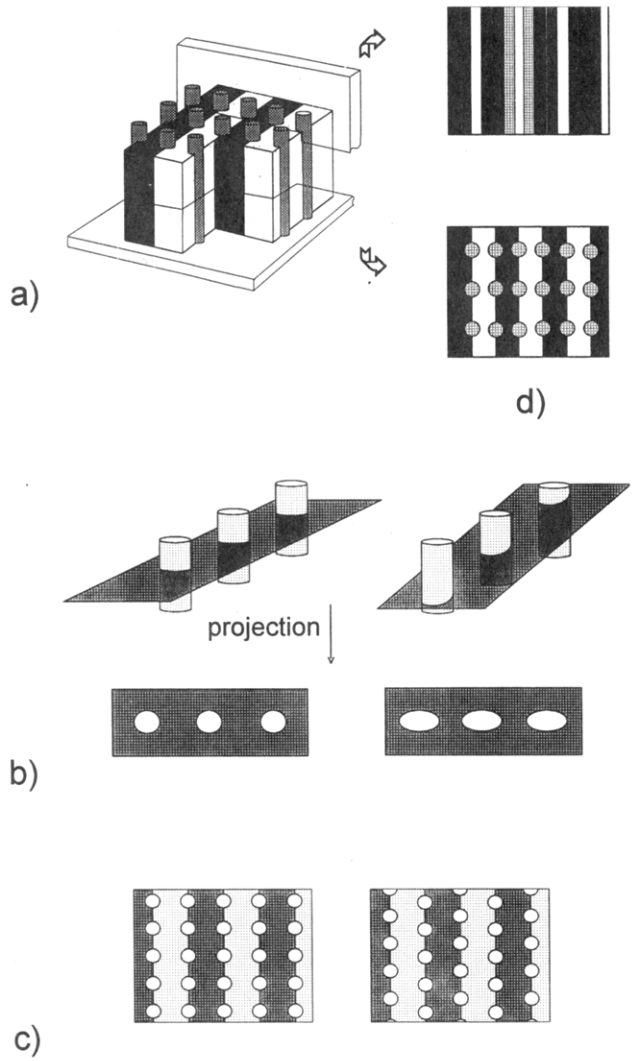

Figure 3. Schematic representations of the (*lc*)-ABC triblock copolymer morphology: (a) (*lc*) morphology realized in SEBM17 and SBM17; (b) schematic representation of an ultrathin section of the (*lc*) morphology showing the B cylinders as regular ellipses at the A/C interface; (c) arrangement of B cylinders at the A/C interface; (d) effect of ultrathin sectioning at different cutting directions on the image formation in the case of the (*lc*) morphology

can be recognized where the section is cut parallel to the cylinders.

A closer analysis of the electron micrographs of SEBM17 shows that the relative arrangement of neighboring cylinder stacks are both directly opposed or staggered (Figure 3c). From the micrograph at large magnification one could conclude that the PEB cylinders are not located symmetrically at the PS/PMMA interface but stick more in the PS lamellae. However this may be a consequence of the staining conditions. Because of the weak incompatibility between PS and PMMA the PS/PMMA interface is relatively broad. Anastasiadis et al. determined an interfacial thickness in P(S-*b*-MMA) diblock copolymers of about 5 nm.[53] If this interface is stained too, the PS lamellae appear broader. TEM micrographs of symmetric P(S-*b*-MMA) diblock copolymers stained with RuO_4 support this interpretation.[54] The dimensions for the different phases are also given in Table 2.

The molecular weight of the PS block in SEBM17 is 100k. For symmetric P(S-*b*-MMA) diblock copolymers this would correspond to a PS lamellar thickness of 33 nm. This compares reasonably to the observed value of 35−40 nm.

Similar micrographs of an ABC triblock copolymer have been reported by Kotaka et al.[37] in 1984 without recognizing the basic structural principle.[55]

The same (lc) morphology is obtained for the nonhydrogenated sample SBM17 (see the micrographs in Figure 2c−e). In Figure 2c, the ultrathin section was treated with RuO_4. The micrograph shows the overall lamellar morphology. Because both PS and PB are stained, the existence of the PB cylinders can only be recognized in some areas of the micrographs.

However, selective staining is possible with OsO_4 (micrographs in Figure 2d,e). Owing to the fact that there is some staining of the PS lamellae by OsO_4, both the lamellar PS/PMMA structure and the PB cylinders located at the PS/PMMA interface can be recognized. Different cylinder orientations with respect to the cutting direction can be determined, as is shown schematically in Figure 3d. Again there is no obvious correlation between the PB cylinders located at neighboring PS/PMMA interfaces. As in the case of SEBM17, the PB cylinders appear to be imbedded more into the PS lamella in SBM17.

From the micrographs the following dimensions of the (lc) morphology are obtained (see also Table 2). The overall lamellar long period is only $L_{lc} \approx 44$ nm. The distance between the cylinders along the lamellar interface is $D_{lc} \approx 25-30$ nm. From the composition the diameter of the cylinders can be calculated to be 11 nm, which is in agreement with the dimensions estimated from the micrographs. This calculation is based on the assumption that the distance between the cylinders is about half the overall long period.

As in the case of the block copolymer with the higher fraction of elastomeric center block, the dimensions of the hydrogenated SEBM17 are considerably larger than that of SBM17. The differences in the long periods are larger than predicted from the variation of the interaction parameter upon hydrogenation (see below).

While hydrogenation of SBM38 and SBM17 does not change the overall morphology, a change in the morphology is observed upon hydrogenation of SBM6, the block copolymer with the very short center block. The polybutadiene block has a molecular weight of only 13.5 k. As expected, the system forms a lamellar morphology type in the case of SBM6. Figure 4a shows the electron micrograph at a low magnification for an ultrathin section stained with RuO_4. The $CHCl_3$ cast and annealed system shows homogeneous ordered lamellae over more than 10 μm. The long period is about 52 nm. Figure 4b shows a micrograph of SBM6 using OsO_4 as the staining agent. The polybutadiene block located at the phase boundary between the polystyrene and the poly(methyl methacrylate) block is strongly stained, while the PS lamellae only show a weak contrast with respect to the PMMA lamella. In contrast to SBM17, where the butadiene block forms cylinders, the polybutadiene block forms isolated entities, most probably spheres at the PS/PMMA interface (Figure 5a). This can be recognized in those areas of the micrograph where the ultrathin section is not perpendicular to the lamella but cuts the lamellar stacks at an angle <90°, as shown in Figure 5b.

Due to the small size of the PB particles with respect to the thickness of the ultrathin section (distance between the PB microdomains ~18 nm; estimated size from the micrograph ~9 nm; calculated size from

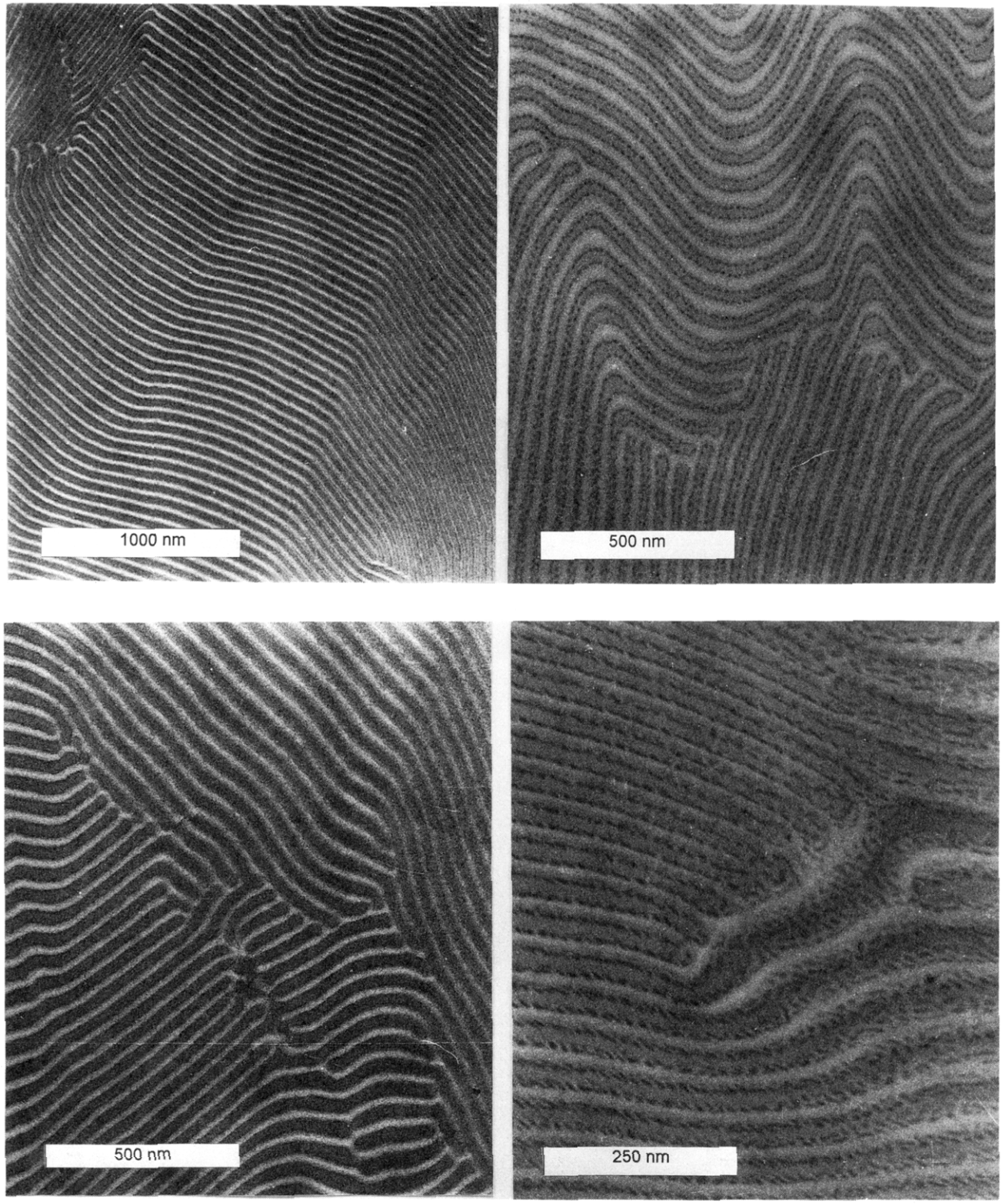

Figure 4. Electron microscopic analysis of SBM6: (a, top left) SBM6, stained with RuO_4 at low magnification; (b, top right) SBM6, stained with OsO_4 at low magnification; (c, bottom left) SBM6, stained with RuO_4 at high magnification; (d, bottom right) SBM6, stained with OsO_4 at high magnification.

composition ~10 nm), the shape cannot be identified unambiguously. However the polybutadiene domains most likely have a spherical or ellipsoidal shape and we will describe this "ball at the wall" morphology[45] as *lamellar-spherical* (ls) structure in the following. Qualitatively, the transition from (lc) to (ls) can be explained as a rupture of the PB cylinders into isolated droplets when the amount of PB is reduced.

In contrast to the lamellar morphology of SBM6, the corresponding hydrogenated block copolymer SEBM6 shows an unexpected cylindrical morphology, in which PS cylinders are dispersed in a PMMA matrix, despite the fact that the PS fraction is 45 wt % (Figure 6a,b).[44] The micrograph with the lower magnification (Figure 6a) shows that the cylindrical morphology is present throughout the sample. There is no indication of a lamellar-type structure. In those areas where the cylinders are cut perpendicular to the cylinder axis it

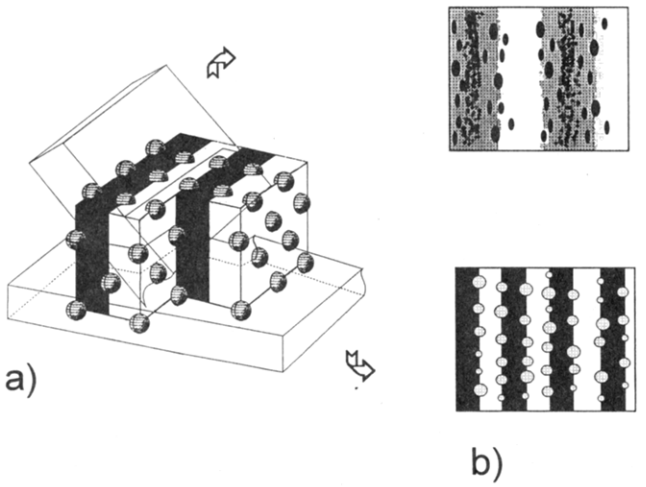

Figure 5. Schematic representations of the (*ls*)-ABC triblock copolymer morphology: (a) (*ls*) morphology realized in SBM6; (b) effect of ultrathin sectioning at different cutting directions on the image formation in the case of the (*ls*) morphology.

can be seen that the cylinders are essentially packed hexagonally. The cylinder long period is ≈60 nm (see Table 2).

Only at very high magnifications can the hydrogenated polybutadiene be recognized as small circular or ellipsoidal objects at the PS/PMMA boundary (Figure 6b). Due to the size of these objects (diameter: 5−10 nm) in comparison to the ultrathin section (thickness around 50 nm) the arrangement of the PEB domains can be recognized only at some areas. If the cut is parallel to the cylinder axis, the PEB domains are recognized as regular circles. If the PEB would form spherical objects such a regular arrangement is not expected. The two-dimensional projection of the micrograph can be explained by the formation of rings surrounding the cylinders, as is shown in Figure 7a. The presence of the PEB microdomains can also be recognized, if the cylinders are cut at an angle below 90°. As demonstrated in Figure 7b and can be seen at larger magnifications of the electron micrographs, the two-dimensional projection results in the observation of ellipsoidal objects. Thus the morphology which can be assigned to SEBM6 is shown in Figure 7c: The polystyrene cylinders are surrounded by the PEB rings.[44] We will describe this structure as (cr) morphology.

The dimensions obtained from the micrographs are as follows: The cylinder long period L_{cr} is about 55−60 nm. The PS cylinders have a diameter of about 35−40 nm. Most probably, the true diameter of the cylinders is slightly below this value because the broad PS/PMMA interface again will be stained by RuO_4. Thus the real cylinder diameter will be on the order of 30−35 nm, which is a reasonable value for a PS chain length of 80k. The PEB rings have a distance D_{cr} along the cylinder axis of 20−25 nm; their diameter R_B can be estimated to be in the range of around 5−8 nm.

As in the case of SEBM17 the morphology of SEBM6 shows the formation of isolated PEB microdomains at the PS/PMMA interface. It is surprising that SEBM6 shows no evidence of a lamellar structure, while SBM6 is purely lamellar. Without the 14k PEB block a lamellar morphology is expected. Obviously, the incorporation of the PEB block (i.e. the hydrogenation of the 1,2-PB block) causes the change in the block copolymer morphology.

B. Thermodynamic Description of Symmetric ABC Triblock Copolymers. In the present section we give a simple theoretical description of symmetric ABC triblock copolymers based on a Flory-type approach originally developed by de Gennes, Alexander, and Semenov[10,11,12,24] for polymer brushes and diblock copolymers.

We attempt to explain the development of A/C interfaces and the sensitivity of the morphology in ABC block copolymers to small changes in composition and the

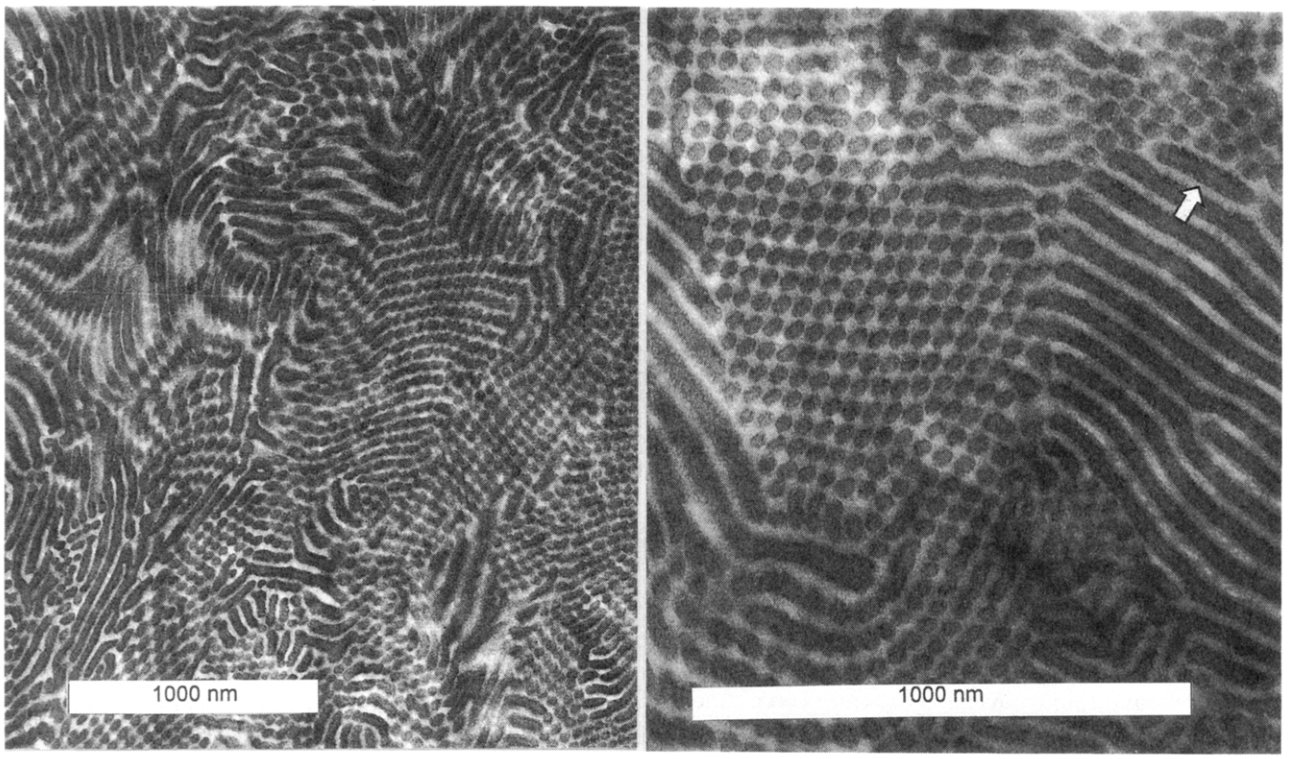

Figure 6. Transmission electron micrographs of SEBM6, stained with RuO_4: (a, left) overview at low magnification; (b, right) enlarged magnification. The arrow indicates the position of the PEB cylinders.

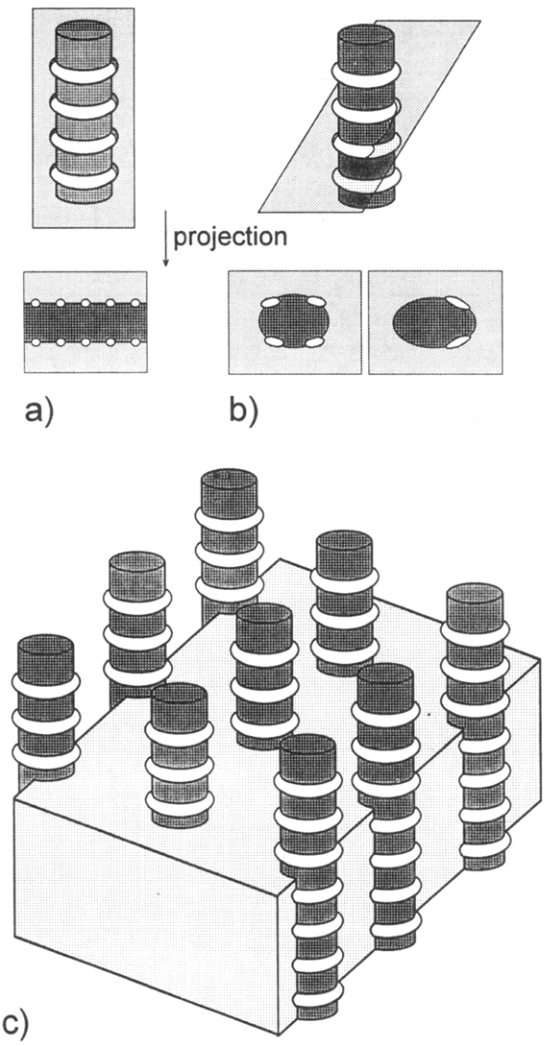

Figure 7. Morphological analysis of SEBM6 based on TEM: (a) representation of circular objects observed along the PS cylinders if the section is parallel to the cylinder axis; (b) ellipsoidal objects observed around the PS cylinders if the section is nearly perpendicular to the PS cylinder axis; (c) schematic representation of the (*cr*) morphology.[40]

thermodynamic imbalance as observed for the morphological transition from (ls) to (cr).

In this approach to describe block copolymers in the strong segregation limit only the contributions of the surface energy and the elastic energy are considered in the formulation of the free energy, neglecting the effects of a finite interface width or contributions resulting from the packing of the microdomains into an ordered "crystal" lattice. The balance of the surface free energy and the elastic potential of the confined chain determines the long spacing under the condition of constant homogeneous segment density and constant overall weight (degree of polymerization N_{tot}, P_n). The morphologies differ in the surface free energies and the elastic energies imposed by chain stretching. In binary AB or ABA block copolymers the composition is the main factor determining the morphology. Only in the weak segregation limit will different morphologies be stable at the same composition (at different interaction energies χN).[21,56]

The same concepts can be applied to ABC triblock copolymers. However, in contrast to the systems where only one binary interaction parameter and one composition variable has to be taken into account to calculate the surface free energy, the ABC system is characterized by two independent composition variables and by three interaction parameters χ_{AB}, χ_{BC}, and χ_{AC} or the respective surface tensions γ_{AB}, γ_{BC}, and γ_{AC}. According to Helfand[7] the interfacial tension γ_{xy} in the strong segregation limit is related to the χ parameter according to

$$\gamma_{xy} \sim (\chi_{xy})^{1/2} \tag{1}$$

In the recent experimental work of Mogi et al.[40,41] and the corresponding theoretical work of Ohta et al.[48] symmetric ABC block copolymers ($\phi_A \approx \phi_C$) in which *B* is the major component ($\phi_B > 0.33$) were considered. The present study focuses on symmetric systems in which B is the minor component ($\phi_B < 0.38$).

As can be seen from the electron micrographs discussed above, A/C interfaces are formed despite the fact that no A−C junctions are present. In addition, as the comparison of SBM6 and SEBM6 shows, hydrogenation is able to switch the morphology. Hydrogenation is equivalent to a change in the interaction parameters χ_{AB} and χ_{BC} *and* the segment length of the B block a_B.

The calculation of the free energy of morphologies as shown in Figures 3 and 5 requires the evaluation of the configurational entropy of the chain in the confinement of these geometries.

The free energy per chain (F_c/kT) in the strong segregation limit at the present level of analysis can be written as

$$\frac{F_c}{kT} = \frac{F_c^{surf}}{kT} + \frac{F_c^{elastic}}{kT} \tag{2}$$

where F_c^{surf} is the contribution of the surface free energy and $F_c^{elastic}$ is the elastic contribution. The surface contribution is given by

$$\frac{F_c^{surf}}{kT} = \gamma_{AB}\Sigma_{AB} + \gamma_{BC}\Sigma_{BC} + \gamma_{AC}\Sigma_{BC} \tag{3}$$

where Σ_{xy} are the common contact areas of component x and y per chain, experiencing the surface tension γ_{xy}. In this notation the surface tensions have the dimension [area]$^{-2}$.

The elastic contribution is given by the elastic retractive force of Gaussian chains and can be written according to

$$\frac{F_c^{elastic}}{kT} = k_A\frac{L_A^2}{N_A a_A^2} + k_B\frac{L_B^2}{N_B a_B^2} + k_C\frac{L_C^2}{N_C a_C^2} \tag{4}$$

where N_A, N_B, and N_C are the number of Kuhn segments (monomer units) of length a_A, a_B, and a_C of the three components. L_A, L_B, and L_C characterize a molecular stretching of A, B, C subchains and k_i (i = A, B, C) is the "force constant" of the different subchains. L_A, L_B, and L_C as well as the values of k_i depend on the morphology of the system.

One of the assumptions of this simple approach is that the gradient of the elastic potential acts normal to the A/B and B/C polymer/polymer interfaces. While this assumption may still be valid in the case of the (ll) morphology (Figure 8a), it only can be a first assumption in the case of the (lc, (ls), and (cr) morphologies. This assumption implies that the distance between the cylinders (D_{lc} in Figure 8b), spheres (D_{ls} in Figure 8c), and rings (D_{cr} in Figure 8d) will be on the order of half

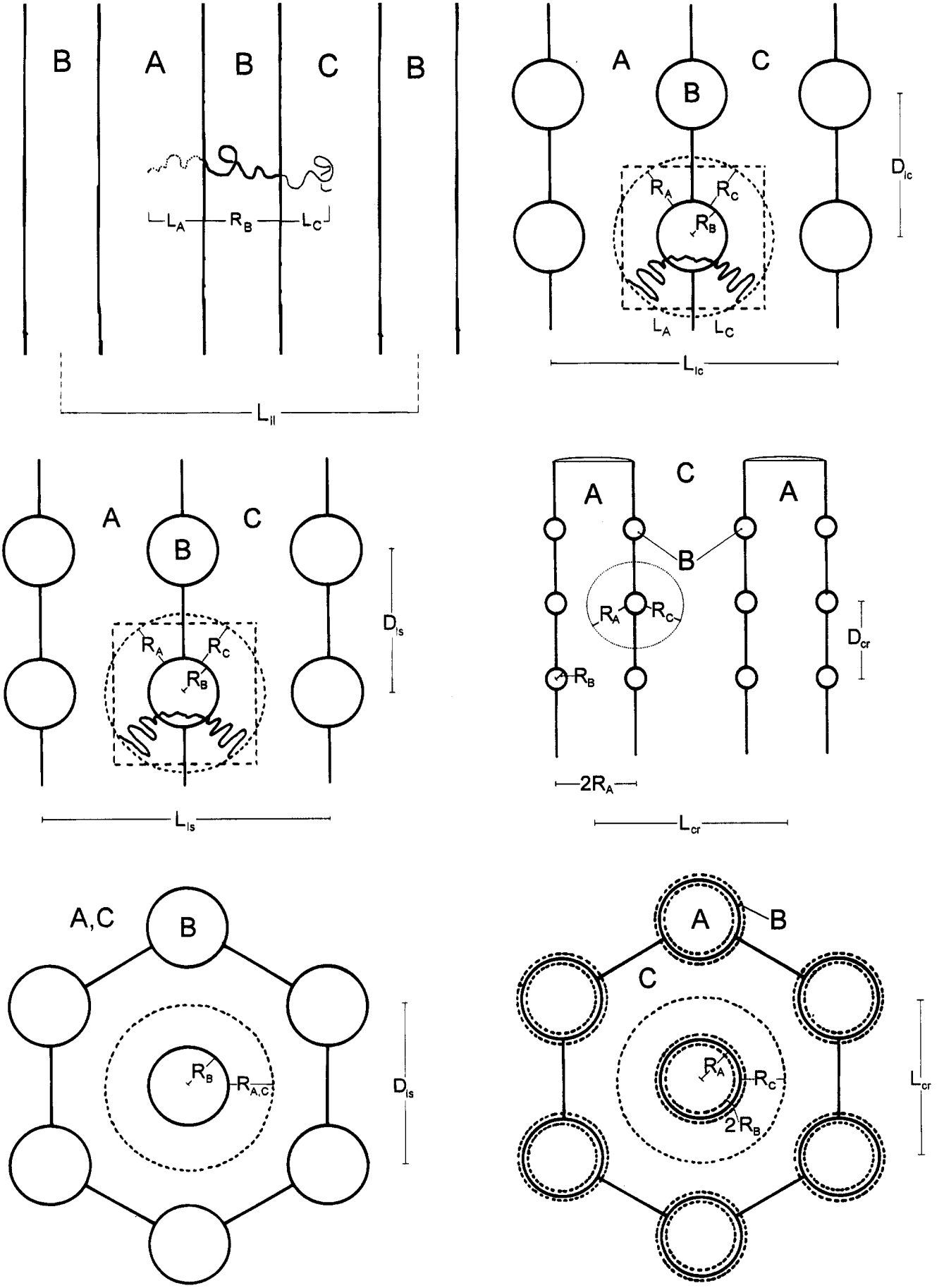

Figure 8. Characteristic dimensions used in the calculation of the free energy: (a, top left) (*ll*) morphology; (b, top right) (*lc*) morphology; (c, bottom left) (*ls*) morphology; (d, bottom right) (*cr*) morphology.

of the long period ($D_{lc} \approx L_{lc}/2$ in Figure 8b; $D_{ls} \approx L_{ls}/2$ in Figure 8c) or twice the radius of the A cylinder ($D_{cr} \approx 2^*R_A$ in Figure 8d). This assumption is in rough agreement with the electron microscopic observations, though the distances normal to the lamellae apparently are slightly smaller than between the cylinders in the case of the (lc) morphology. In a more sophisticated treatment the detailed gradient of the elastic potential which may be different normal and parallel to the interface should be taken into account. In addition, chain deformation resulting from the packing of the micelles is completely neglected in the present level of approximation.

Using the condition of incompressibility, i.e. maintaining homogeneous segment densities, all unknown quantities (the three Σ_{xy}'s and the molecular deformation parameters L_A, L_B, and L_c can be expressed by only one geometrical parameter if the segmental volumes ν_A, ν_B, and ν_C and the volume fractions ϕ_A, ϕ_B, and ϕ_C are known, using the relation

$$\phi_i = \frac{N_i \nu_i}{\sum_{A,B,C} N_i \nu_i} \tag{5}$$

In the present work all unknowns are expressed by the geometrical quantity describing component B, i.e. R_B which is the thickness of the B lamellae in (ll), the radius of the B cylinders in (lc), the radius of the spheres in (ls), and the radius of the B rings in (cr).

In all cases the equation of the free energy per chain (eq 2) takes the form

$$\frac{F_c}{kT} = \frac{N_B \nu_B}{R_B} K_m^{surf} + \frac{R_B^2}{N_B} K_m^{elastic} \tag{6}$$

where K_m^{surf} is a morphology dependent function (m = (ll), (lc), (ls), (cr)) which only depends on the surface tensions γ_{xy} and ϕ_B. $K_m^{elastic}$ also is a morphology dependent function which depends on the segmental volumes ν_A, ν_B, and ν_C, the Kuhn step length a_A, a_B, and a_C, and the volume fractions ϕ_A, ϕ_B, and ϕ_C. It also takes into account inhomogeneous chain stretching.

Minimization of the free energy with respect to R_B gives

$$R_B^{min} = \left(\frac{\nu_B K_m^{surf}}{2 K_m^{elastic}} \right)^{1/3} N_B^{2/3} \tag{7}$$

As for AB diblock copolymers the characteristic dimensions (long period, cylinder or sphere distance, and diameter) scale as $N^{2/3}$. This is a consequence of the symmetric elastic potential assumed in the calculation (see above).

To evaluate the stability limits of the different morphologies, the minimum free energies have to be compared

$$\frac{F_{c(m)}^{min}}{kT} = N_B^{1/3} (K_m^{surf} \nu_B)^{2/3} (K_m^{elastic})^{1/3} 3/2 \cdot 2^{1/3} \tag{8}$$

The relative contributions of the surface energy and the elastic energy at the minimum are (2:1).

Table 3 summarizes the functions K_m^{surf} and $K_m^{elastic}$ for the different morphologies at the present level of approximation.

Table 3. Functions Entering the Equation of the Free Energy

morphology	K_m^{surf}	$K_m^{elastic}$
(ll)	$\gamma_{AB} + \gamma_{BC}$	$\frac{3}{2}\left[\frac{N_B}{N_A a_A^2}\left(\frac{\phi_A}{\phi_B}\right)^2 + \frac{1}{a_B^2} + \frac{N_B}{N_c a_c^2}\left(\frac{\phi_c}{\phi_B}\right)^2\right]$
(lc)	$\gamma_{AB} + \gamma_{BC} + \gamma_{AC}\left(\frac{1}{(\pi\phi_B)^{1/2}} - \frac{2}{\pi}\right)$	$\frac{3\pi^2}{8a_B^2} + \frac{3}{2}\frac{\nu_A}{\nu_B a_A^2}\ln\left(1 + 2\frac{\phi_A}{\phi_B}\right)^{1/2} + \frac{3}{2}\frac{\nu_C}{\nu_B a_C^2}\ln\left(1 + 2\frac{\phi_C}{\phi_B}\right)^{1/2}$
(ls)	$\frac{3}{2}\gamma_{AB} + \frac{3}{2}\gamma_{BC} + \frac{3}{4\pi}\left(\frac{2}{\sqrt{3}}\pi^{2/3}\phi_B^{-2/3} - \pi\right)\gamma_{AC}$	$\frac{1}{2}\frac{\nu_A}{a_A^2 \nu_B}\left(1 + \left(1 + \frac{\phi_A}{\phi_B}\right)^{-1/3}\right) + \frac{8}{3a_B^2} + \frac{1}{2}\frac{\nu_C}{a_c^2 \nu_B}\left(1 + \left(1 + \frac{\phi_C}{\phi_B}\right)^{-1/3}\right)$
(cr)	$\left(\frac{\left(\frac{\phi_A}{\phi_B}\pi - 1\right)^{1/2} - 1}{2\pi^2}\right)\left(\gamma_{AB} + \gamma_{BC} + \gamma_{AC}\right)$	$\frac{3}{8}\pi^2\frac{1}{a_B^2} + \frac{\nu_A}{a_A^2 \nu_B}\ln\left(2 + \frac{2}{\pi^{1/2}}\frac{\left(\frac{\phi_A}{\phi_B}\pi - 1\right)^{1/2}}{qq}\right) + \frac{3\nu_C}{2a_C^2 \nu_B}\left(1 - \frac{1}{1 + \frac{2}{\pi^{1/2}}\frac{bb}{qq}\left(\left(\frac{\pi}{\phi_B}\right)^{1/2} - qq\right)^{1/2}}\right)$ $qq = \left(\frac{\phi_A}{\phi_B}\pi - \frac{1}{2}\right)^{1/2}$

Table 4. Surface Tensions, Solubility Parameters, and χ Parameters of the SBM and SEBM System

polymer pair	interfacial tensions, dyn/cm[a]	cohesive energy density, $(\delta_A - \delta_B)^2$, J/cm^3 [b]	interaction parameter χ_{AB}[c]
PS/PB		0.49	0.045
PS/PEB	5.7	1.21	0.112
PS/PMMA	1.3[e]	0.04	0.0044
PMMA/PB		0.81	0.071
PMMA/PEB	9.5	1.69	0.147
f_{SBM}[d]		0.125	0.14
f_{SEBM}[d]	0.085	0.083	0.092

[a] Surface tensions taken at 150 °C; because of the lack of data for PEB the data for polyethylene are used. Reference: Wu, S. In *Polymer Handbook*, 3rd ed.; Brandrup, J., Immergut, E. H., Eds.; J. Wiley & Sons: New York, 1989; Chapter VI, p 411. [b] Because $\gamma \propto \chi^{1/2}$ and $\chi \propto (\delta_A - \delta_B)^2$ it follows that $\gamma \propto |\delta_A - \delta_B|$ with some corrections taking account for differences in the molar segmental volumes $V_{segment}$. Solubility parameters were taken from *Polymer Handbook*, 3rd eds.; Brandrup, J.; Immergut, E. H., Eds.; J. Wiley & Sons: New York, 1989. The following values were used: $\delta_{PS} = 9.1$ (cal/cm^3)$^{1/2}$; $\delta_{PMMA} = 9.3$ (cal/cm^3)$^{1/2}$; $\delta_{PB} = 8.4$ (cal/cm^3)$^{1/2}$; $\delta_{PEB} = 8.0$ (cal/cm^3)$^{1/2}$. Owing to the large variation of the solubility parameters given in the literature, the value of f is suspect to a considerable uncertainty. [c] Calculated from the solubility parameters under the assumption that the molar segmental volumes are given by the geometric mean of the molar volumes of the components according to $\chi_{AB} = (a^3/(kT))(\delta_A - \delta_B)^2$. The interacting area was calculated according to $(V_{segment}/N_A)^{1/3}$. [d] $f = X_{AC}/(X_{AB} + X_{BC})$ with $X = \gamma$, $|\delta_A - \delta_B|$, $\chi^{1/2}$. [e] Value taken from ref 49.

K_m^{surf} has the general form

$$K_m^{surf} = f_{AB}\gamma_{AB} + f_{BC}\gamma_{BC} + f_{AC}(\phi_B^{\beta})\gamma_{AC} \qquad (9)$$

where $f_{AB,BC}$ are constants, depending on the type of morphology and $f_{AC}(\phi_B^{\beta})$ is a function which depends on the morphology and the volume fraction of component B. β describes the power in which the fraction of B enters in $f_{AC}(\phi_B^{\beta})$.

Before discussing the results in some more detail (section B.3), the evaluation of K_m^{surf} and $K_m^{elastic}$ and the problems encountered will be discussed for the (ll) and (lc) morphologies in sections B.1 and B.2. The details of the calculation used to approximate the (ls) and (cr) morphology are given in the appendices.

In the present calculations only situations will be considered where $\Sigma_{AB} = \Sigma_{BC}$, i.e. where the A/B and the B/C contact areas are the same. In a rigorous sense this requires that $\gamma_{AB} = \gamma_{BC}$, which is not strictly valid for the actual SBM and SEBM block copolymers (see Table 4 for surface tensions). As a result of this assumption the B cylinders are located symmetrically between A and C (lc). The same holds for the location of the B spheres (ls). For the (cr) morphology this requires that the radius of the ring R_B in (cr) be small compared to the cylinder radius R_A (which only will be valid for low volume fractions of B). The condition $\Sigma_{AB} = \Sigma_{BC}$ not only requires that the surface tensions $\gamma_{AB} \approx \gamma_{BC}$ be similar, but also the volume fractions of components A and C (i.e. $\phi_A = \phi_C$). If this is not the case, the system will tend to create different contact areas between A/B and B/C which would result in a curved morphology type. Thus cylindrical morphologies could be induced not only by asymmetric compositions but also by the asymmetry of the A/B and B/C interaction. This is a fundamentally different feature of ABC triblock copolymers in comparison to AB or ABA block copolymers.

It has been mentioned in the introduction that Mogi et al.[40] observe a lamellar ABC morphology for a symmetric ($\phi_A = \phi_B = \phi_C$) triblock copolymer of the sequence polyisoprene-*block*-polystyrene-*block*-poly(vinylpyridine)) (ISVP). In terms of the solubility parameters polystyrene (S) is intermediate between polyisoprene (I) and poly(vinylpyridine) (VP). As a consequence the surface tension $\gamma_{I-S} \approx \gamma_{S-VP}$ should be not be too dissimilar and we would predict from our calculations a lamellar morphology. If the block sequence is changed as in the system studied by Thomas et al.,[43] having the sequence polystyrene-*block*-polyisoprene-*block*-poly(vinylpyridine) (SIVP), the situation is different. Because $\gamma_{I-VP} \gg \gamma_{S-I}$, the system will tend to create a large S/I contact area which allows the reduction of the stretching of PS (and PI) chains and a small I/VP contact area to reduce the very unfavorable contacts between these highly immiscible polymers. As a result of this imbalanced A/B and B/C interaction a core–shell morphology with a poly(vinylpyridine) core forms. Such core–shell type morphologies will not be considered in the present paper, but it is evident from these qualitative considerations that switching the block sequence can change the morphology even if the composition would favor a lamellar microdomain structure. In very recent work Birshtein et al.[50] arrived at the same conclusion.

The (cr) morphology observed in SEBM6 may also be an example of such a situation because the PMMA block is slightly longer. It is evident that the condition $\gamma_{AB} \approx \gamma_{BC}$ is also not valid for the SBM and SEBM systems though it may be not as severe as in the S/I/VP system. A more elaborate theory should take this nonsymmetry of the interactions into account.

B.1. ABC Lamellae (ll). The lamellar ABC block copolymer (ll) can be treated in analogy to lamellar AB diblock copolymers as a first approximation. We assume homogeneous chain stretching of the blocks L_A, L_B, and L_C. If the B chain is stretched homogeneously, the thickness of the B lamellae R_B is equal to the stretching L_B.

From the condition of homogeneous segment density it follows

$$N_B\nu_B = \Sigma_{AB}R_B = \Sigma_{BC}R_B \qquad (10a)$$

$$N_A\nu_A = \Sigma_{AB}L_A \qquad (10b)$$

$$N_C\nu_C = \Sigma_{BC}L_C \qquad (10c)$$

From (10a) it follows that the contact areas must be identical $\Sigma_{AB} = \Sigma_{BC}$ in a lamellar morphology neglecting local fluctuations. Because no AC interface exists in a (ll) morphology eq 3 becomes

$$\frac{F_{c(ll)}^{surf}}{kT} = \frac{N_B\nu_B}{R_B}(\gamma_{AB} + \gamma_{BC}) \qquad (11)$$

According to eq 10, the stretching of A and C chains (L_A, L_C) can be expressed in terms of the stretching of B chains, and thus the elastic contribution to the free energy (eq 4) can be written as a function of R_B according to

$$\frac{F_{c(ll)}^{elastic}}{kT} = \frac{3}{2}\frac{R_B^2}{N_B}\left[\frac{N_B}{N_A a_A^2}\left(\frac{\phi_A}{\phi_B}\right)^2 + \frac{1}{a_B^2} + \frac{N_B}{N_C a_C^2}\left(\frac{\phi_C}{\phi_B}\right)^2\right] \qquad (12)$$

The overall long period L_{ll} is

$$L_{ll} = 2\frac{R_B}{\phi_B} \tag{13}$$

B.2. B Cylinders at the A/C Interface (lc). This morphology represents a combination of a cylindrical morphology and a lamellar morphology. According to Figure 8b we define a subcell of the dimensions $(l_A + l_B)^* D_{lc}^* h$ which contains Q chains in one cylinder of height h. In contrast to hexagonally packed cylinders, where a Wigner–Seitz cell is appropriate to describe the arrangement of the micelles, the symmetry of the ABC block copolymer will not allow the packing according to a hexagonal Wigner–Seitz cell.

Thus the following relations hold if the cylinder is symmetrically located at the A/C interface:

$$h\pi R_B^2 = QN_B\nu_B \tag{14}$$

and

$$\Sigma_{AB}Q = h\pi R_B = \Sigma_{BC}Q$$

$$\Sigma_{AB} = \Sigma_{BC} = \frac{N_B\nu_B}{R_B} \tag{15}$$

From the overall A/C interface in a subcell and the number of chains Q the A/C contact area per chain is given by

$$\Sigma_{AC} = \left(\frac{D_{lc}}{R_B} - 2\right)\frac{N_B\nu_B}{\pi R_B} \tag{16}$$

As has been discussed above the experimental data on SBM17 and SEBM17 indicate that the stretching of A and C chains normal and parallel to the lamellar interface is about the same. We make the following approximation for the relation between the lamellar long period L_{lc} and the distance between the cylinders D_{lc}:

$$L_{lc} = 2(l_A + l_B) = 2D_{lc} \tag{17}$$

Thus Σ_{AC} is given by

$$\Sigma_{AC} = \frac{N_B\nu_B}{R_B}\left(\frac{1}{(\pi\phi_B)^{1/2}} - \frac{2}{\pi}\right) \tag{18}$$

This equation is valid for systems where $\phi_A = \phi_C$. For slight asymmetries some correction to eq 17 may be applied.

Thus the surface energy part for the (lc) morphology is given by

$$\frac{F_{c(lc)}^{surf}}{kT} = \frac{N_B\nu_B}{R_B}\left(\gamma_{AB} + \gamma_{BC} + \gamma_{AC}\left(\frac{1}{(\pi\phi_B)^{1/2}} - \frac{2}{\pi}\right)\right) \tag{19}$$

The description of the elastic potential is much more problematic. For AB diblock copolymers Semenov[12] calculated the elastic free energy of the core of spherical and cylindrical morphologies. The problem is to maintain a homogeneous segment density in the core at the lowest average deformation of the chains in the core. Semenov's result is only valid for diblocks, in which one end of the block is located at the surface of the microdomain and the other is located within the microdomain. From symmetry arguments ABA triblock with cylindrical B domains can be described as A–(B/2) chains. However this is not possible anymore for ABC block copolymers where the two ends will have to leave the cylinder on opposite sides. Qualitatively, we expect a higher elastic potential than the Semenov result for cylindrical micelles. This problem of a higher stretching of the B chains in ABC block copolymers has also been recognized by Spontak et al. for a lamellar (ll) morphology.[49]

If the area Σ_{AB} is the same for all chains, the average length of a B chain $\bar{L}_B$ entering the domain at the A/B interface and leaving at the B/C interface may be estimated as

$$\bar{L}_B = \frac{\int_0^{R_B} 2\pi r\, dr}{2R_B} = \frac{\pi}{2}R_B \tag{20}$$

The elastic potential of the B chains thus may be written as

$$\frac{F_{c(B)}^{elastic}}{kT} = \frac{3}{2}\frac{L_B^2}{N_B a_B^2} = \frac{3\pi^2}{8}\frac{R_B^2}{N_B a_B^2} \tag{21}$$

This result can be compared to that obtained by Semenov for the cores of a cylinder in a AB diblock[12,24] (for chains of length $N_B/2$).

$$\frac{F_{c(B)}^{elastic}}{kT} = \frac{\pi^2}{8}\frac{R_B^2}{N_B a_B^2} \tag{22}$$

The A and C chains each form half of the corona surrounding the B cylinder. The corresponding equivalent radii (R_A, R_C) are given by

$$R_A = R_B\left[\left(1 + 2\frac{\phi_A}{\phi_B}\right)^{1/2} - 1\right]$$

$$R_C = R_B\left[\left(1 + 2\frac{\phi_C}{\phi_B}\right)^{1/2} - 1\right] \tag{23}$$

To describe the elastic free energy of the A and C chains the inhomogeneous stretching of chains must be taken into account according to refs 10 and 12. For the (lc) morphology the resulting equations for the elastic potential are

$$\frac{F_{c(A)}^{elastic}}{kT} = \frac{3}{2}\frac{R_B^2\nu_A}{N_B\nu_B a_A^2}\ln\left(1 + \frac{R_A}{R_B}\right) \tag{24}$$

$$\frac{F_{c(C)}^{elastic}}{kT} = \frac{3}{2}\frac{R_B^2\nu_C}{N_B\nu_B a_C^2}\ln\left(1 + \frac{R_C}{R_B}\right) \tag{25}$$

The total elastic potential for (lc) thus is given by

$$F_{c(lc)}^{elastic} = \frac{R_B^2}{N_B}\left[\frac{3\pi^2}{8a_B^2} + \frac{3}{2}\frac{\nu_A}{\nu_B a_A^2}\ln\left(1 + 2\frac{\phi_A}{\phi_B}\right)^{1/2} + \frac{3}{2}\frac{\nu_C}{\nu_B a_C^2}\ln\left(1 + 2\frac{\phi_C}{\phi_B}\right)^{1/2}\right] \tag{26}$$

The treatment of the two other morphologies considered in this work follows the same lines (see appendices).

As a consequence of the inhomogeneous stretching of the A and C chains, the elastic contribution is strongly

influenced by the behavior of the B chains even if they are only present in a minor amount. This is even more pronounced in the case of the (ls) morphology (see Appendix I).

B.3. Results of Model Calculations. In the model calculations the following parameters have been used. The segmental volumes $v_{A,B,C} = a_{A,B,C}^3$ and Kuhn length $a_{A,B,C} = 0.5$ nm where kept the same for the three components. The degree of polymerization P_n was $N_{tot} = 1000$. The volume fraction of B was varied between 0.4 and 0.01, keeping the volume fractions of A and C constant.

$$\phi_A = \phi_C = \frac{1 - \phi_B}{2} \tag{27}$$

For very small volume fractions of B the assumption of strong segregation, i.e. sharp phase boundaries, is not valid anymore. In the limit of strong segregation, the molecular weight has no influence on the "phase diagram". The main focus of the present discussion will be related to the influence of the imbalance of the thermodynamic interactions on the morphologies.

Parts a–c of Figure 9 show the results of calculations of the minimum of the free energy for the different morphologies for three sets of interaction parameters (surface tensions). If $\gamma_{AC} = \gamma_{AB} = \gamma_{BC}$ (Figure 9a) the lamellar ABC morphology (ll) has the lowest free energy down to a volume fraction of $\phi_B \approx 0.05$. At lower volume fractions a transition to the (lc) morphology is predicted. The other two morphologies (ls) and (cr) always have a higher free energy.

If the surface tension γ_{AC} becomes smaller (Figure 9b,c) the transition from the (ll) to the (lc) morphology shifts to larger values, and finally, the (ls) and (cr) morphologies can become the most favorable structures at small volume fractions of B.

As can be seen from the analysis of the equations describing the free energy (see also Table 3), a parameter which can be used to describe the relative incompatibilities between the three components independent of the individual parameters is

$$f = \frac{\gamma_{AC}}{\gamma_{AB} + \gamma_{BC}}$$

or the weighted difference of the surface tensions $(1 - f)$. In the calculations either γ_{AC} has been varied by keeping $\gamma_{AB} + \gamma_{BC}$ constant or vice versa. In the limit of strong segregation this makes no difference.

Figure 10 shows the "phase diagram" for the different morphologies considered in this work. $1 - f$ is used as a measure of the relative incompatibility. As can be seen, the model predicts stability windows for all four morphologies considered in the present work.

The value $(1 - f) = 1$ (i.e. $f = 0$) can be achieved either at $\gamma_{AC} = 0$ or at $(\gamma_{AB} + \gamma_{BC}) = \infty$. In the first case the transitions between B lamella, B cylinders, and B spheres should be the same as in an ABA block copolymer. However this is not the case in the present calculations which still assume segregation between A and C. At this end the calculation overestimates the elastic contribution to the free energy because it is limited to strong segregation. If only the surface free energies are considered, the location of the morphological transitions at $(1 - f) = 1$ are the same as for a binary AB block copolymer.

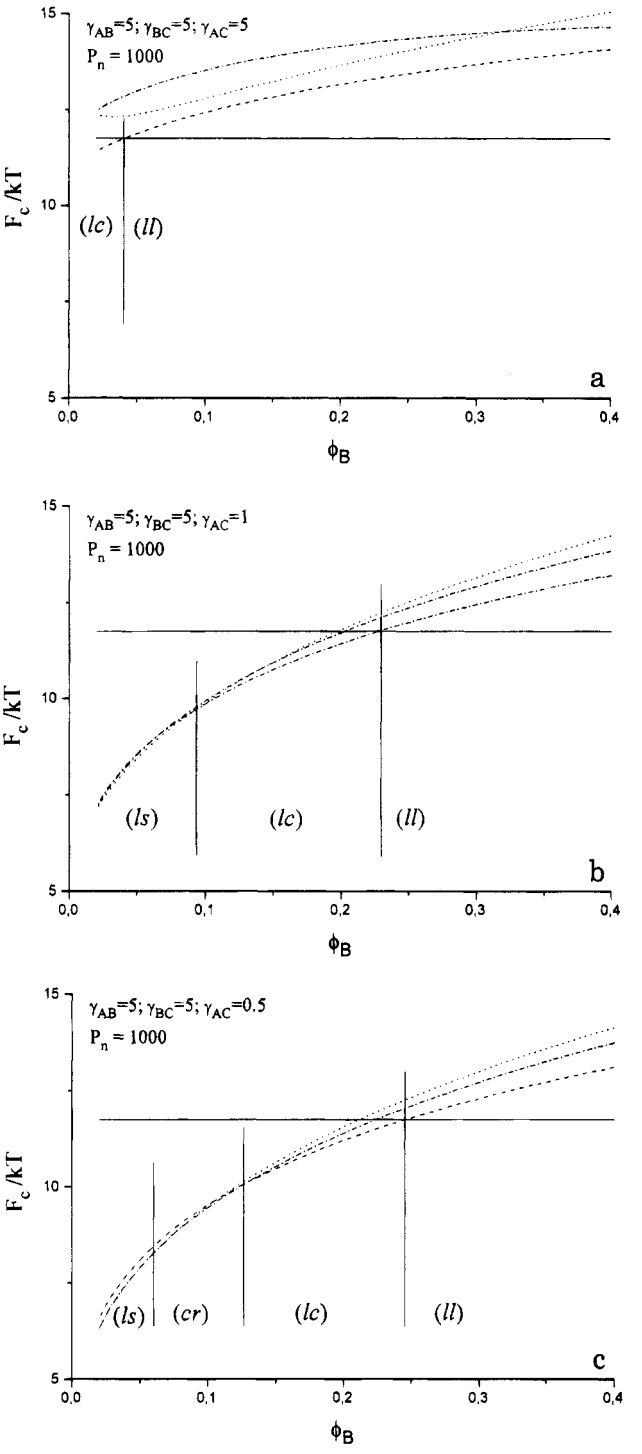

Figure 9. Minimized free energy per chain (F_c/kT) for symmetric ABC triblock copolymers as a function of the volume fraction of the center block ϕ_B for the various morphologies (*ll*), (*lc*), (*ls*), and (*cr*): (a) $\gamma_{AB} = \gamma_{BC} = \gamma_{AC} = 5$ dyn/cm; (b) $\gamma_{AB} = \gamma_{BC} = 5$ dyn/cm, $\gamma_{AC} = 1$ dyn/cm; (c) $\gamma_{AB} = \gamma_{BC} = 5$ dyn/cm, $\gamma_{AC} = 0.5$ dyn/cm.

The second possibility of $1 - f = 1$ is realized if $\gamma_{AB} + \gamma_{BC} = \infty$. A and C are still segregated and thus the estimation of the elastic contribution will be more realistic.

The model predicts that below a certain critical value of $1 - f$ only the (ll) is stable, even at very low B volume fraction. Such a situation is realized if the end blocks (A, C) are highly immiscible and the center block acts as a compatibilizer. We would expect that such a situation could be realized in poly(isoprene)-*block*-polystyrene-*block*-poly(vinylpyridine) or in poly(buta-

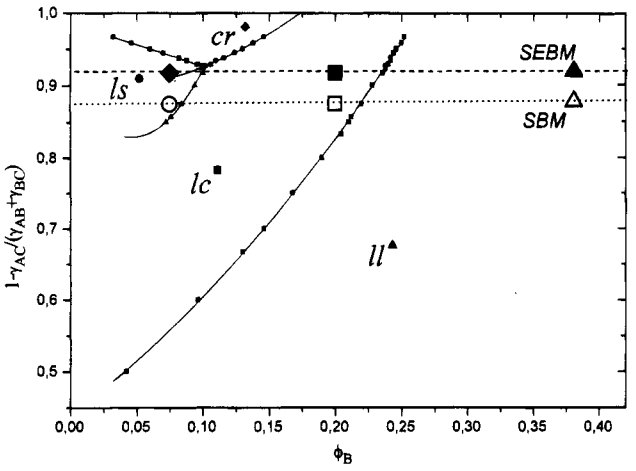

Figure 10. Phase diagram of symmetric ABC triblock copolymers ($\phi_B < 0.4$). (*ll*), (*lc*), (*lc*), and (*cr*) define the stability windows for the various morphologies. Included are the lines describing the situation realized in SBM and SEBM triblock copolymers and the location of the block copolymers SBM6, SEBM6, SBM17, and SEBM 17.

diene)-*block*-polystyrene-*block*-poly(methyl methacrylate). In a range $0.45 \lesssim 1 - f \lesssim 0.8$ the model predicts only one morphological transition (ll) ⟶ (lc). In the range $0.8 \lesssim 1 - f \lesssim 0.9$ two transitions are expected if the B volume fraction is lowered (ll) ⟶ (lc) ⟶ (ls). Above a critical value of $1 - f$ the (cr) morphology has a stability window between the (lc) and (ls) structure. The exact size of the stability window of the (cr) morphology crucially depends on the calculation of the elastic potential used in the free energy calculations. As can be seen in Figure 9, the absolute values of the (ls), (cr), and (lc) morphology differ only slightly in the range of low ϕ_B. The present approximation thus bears some uncertainties with respect to the (cr) stability window.

The most important results which can be extracted from Figure 10 are the following:

• Below a critical value of $(1 - f)$ no (ls) and (cr) morphology can be formed. In the case of $(1 - f) = 1$ the behavior of the ABA triblock copolymers is not achieved because the configuration of the B chains still assumes that the A–B and B–C junctions are located at opposite sides of the B domain.

• Even in the limit of strong segregation morphological transitions can be expected by changes of the interaction parameters (relative imbalance), keeping the composition constant. This change in the interaction may be achieved by a temperature variation or by a slight chemical modification.

Within the limit of the model used in the present paper, the characteristic dimensions scale with the molecular weight according to $M^{2/3}$. In contrast to simple AB block copolymers where the dimensions vary with the surface tension according to $\gamma^{1/3}$ the dependence of the dimensions on the thermodynamic imbalance is more complex.

Figure 11 summarizes some results of model calculations to evaluate the influence of the surface tensions on the microphase dimensions. Figure 11a shows the dependence of the lamellar long period of the (ll) morphology as a function of γ_{AB} using $\gamma_{AB} = \gamma_{BC}$ at fixed γ_{AC} and a B volume fraction of 0.3 where only the (ll) morphology is stable. As expected, the long period scales as $^1/_3$ with the surface tension (more accurately with the sum $\gamma_{AB} + \gamma_{BC}$). In Figure 11b the same plot is shown for a B volume fraction of 0.15. The long period of the (ll) morphology does not depend on the composition. The perpendicular line separates the stability limits of the (ll) and (lc) morphology. In the range where (lc) is more stable, the model predicts a dependence of the (lc) long period which is close to $^1/_3$. The long period of the (lc) morphology is considerably smaller than the long period of an (ll) morphology which is in agreement with the experimental data (see Table 2). Figure 11c shows the results of calculations at $\phi_B = 0.15$ in which the surface tensions γ_{AB} and γ_{BC} were kept constant (=5 dyn/cm). The long period is plotted as a function of f. As expected the (ll) morphology shows no dependence of the long period on f if only γ_{AC} is varied. The variation of L_{lc} is only very small. The same is shown in Figure 11d for $\phi_B = 0.06$, where all morphologies could occur depending on the relative incompatibility.

Included in Figure 10 are the $(1 - f)$ values estimated for the SBM (dotted line) and SEBM (dashed line) block copolymers. Table 4 lists the interfacial tensions, solubility, and interaction parameters of the various binary pairs PS/PMMA, PS/PB, PS/PEB, PMMA/PB, and PMMA/PEB which have been used in the calculation. Again we assume that $\Sigma_{AB} = \Sigma_{BC}$, i.e. we do not take into account that the asymmetry of the interactions also will induce some curvature. The differences between the polybutadiene and the hydrogenated system are evident. The interfacial tension between PEB/PMMA and PEB/PS is much larger than between the less immiscible PS/PMMA or PS/PB pairs.

The large symbols (open and closed) which are included in Figure 10 correspond to the block copolymers used in this study. The volume fractions have been calculated under the assumption that the densities of the components in the block copolymer are the same as the bulk materials.

For SBM block copolymers only the transitions (ll) ⟶ (lc) ⟶ (ls) are expected, and the experimentally observed morphologies of SBM38 (open triangle), SBM17 (open square), and SBM6 (open circle) are correctly predicted by the model. For SEBM block copolymers the model predicts the following morphological transitions if the B volume fraction is reduced:

$$(ll) \longrightarrow (lc) \longrightarrow (cr) \longrightarrow (ls)$$

The experimentally observed morphologies of SEBM38 and SEBM17 again are correctly predicted by the model. For SEBM6 the (cr) morphology is observed. According to the model, SEBM6 is just located at the borderline between the (ls) and (cr) morphology. In light of the crude approximations and the nonperfect symmetry of SEBM6 (both with respect to composition and thermodynamic interactions) we consider the agreement between the model predictions and the experiments as satisfactory.

The surprising observation of a change in the morphology type from a coarse lamellar to a coarse cylindrical morphology is difficult to understand without a theoretical basis. Analyzing the individual contributions to the free energy, we now can argue along the following lines: Hydrogenation enhances the immiscibility of the center B block to the end blocks. The system thus could lower its surface energy either by making larger spheres which would correspond to an increase of the elastic potential of the *B*-chains or by making cylinders. This could be realized in a (lc) morphology. However in a (lc) morphology the A and C chains have a higher elastic potential than in a (ls) morphology. The (cr) morphology obviously represents

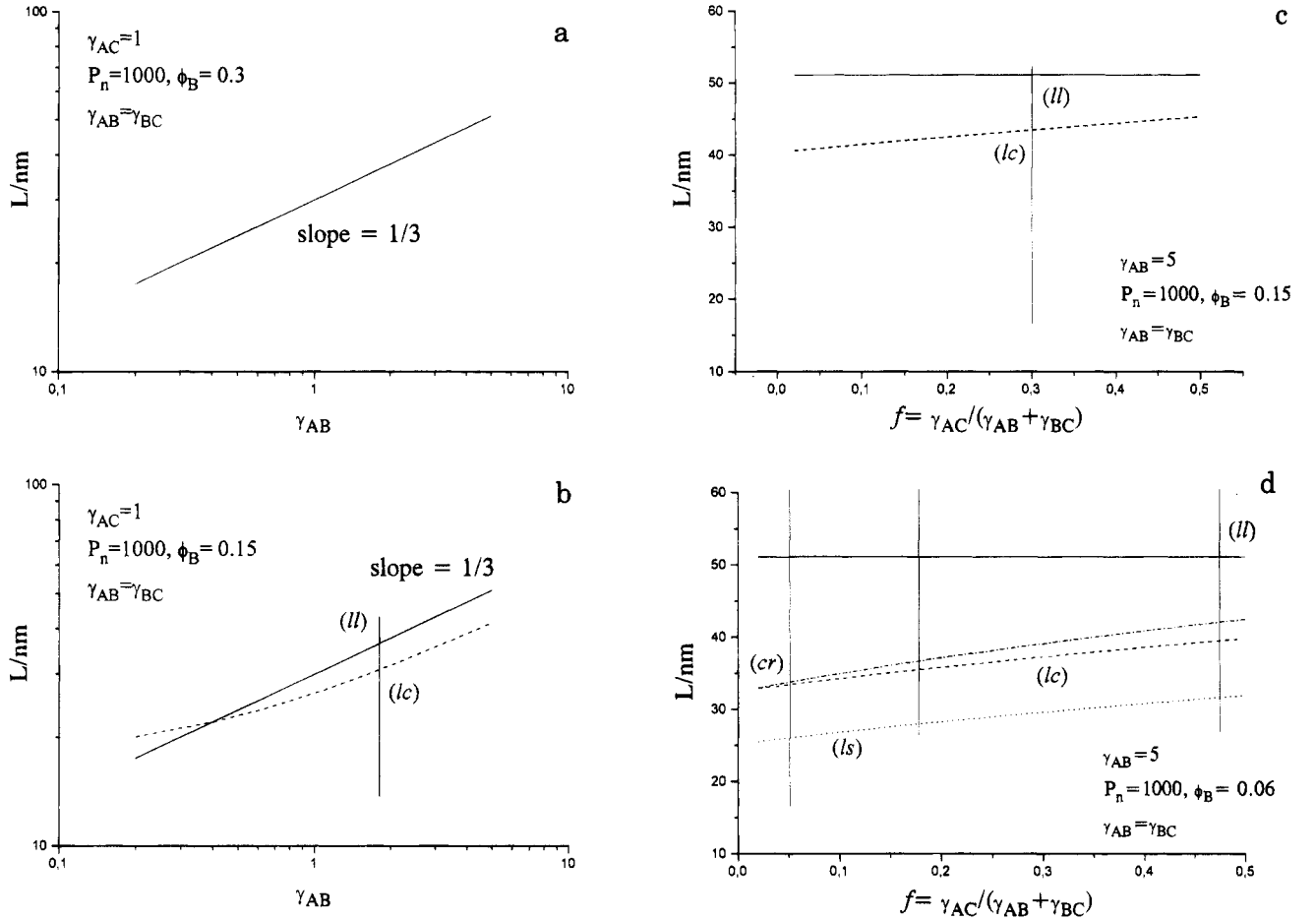

Figure 11. Dependence of the microdomain size on the variation of the surface tensions. The perpendicular lines indicate morphological transitions where appropriate. (a) Variation of the lamellar long period [(*ll*)-morphology] with the A/B, B/C surface tensions, keeping γ_{AC} constant; $\phi_B = 0.3$. (b) Varition of the lamellar long period [(*ll*)-morphology and (*lc*)-morphology] with the A/B, B/C surface tensions, keeping γ_{AC} constant; $\phi_B = 0.15$. (c) Dependence of the lamellar long period [(*ll*)-morphology (full line) and (*lc*)-morphology (- - -)] on the variation of the A/C surface tension, keeping the A/B, B/C surface tensions constant; $\phi_B = 0.15$. (d) Dependence of the long period [(*ll*)-morphology (full line), (*lc*)-morphology (- - -), (*ls*)-morphology (• • •)), (*cr*)-morphology (• – •)] on the variation of the A/C surface tension, keeping the A/B, B/C surface tensions constant; $\phi_B = 0.06$.

an optimum compromise: component B forms small cylinders with the result of a smaller B chain stretching, and C which is present in slight excess (the system is not perfectly symmetrical) forms the matrix and thus the C chains experience only a rather weak elastic potential which resembles that of a corona of a sphere.

Conclusions

The experimental results and calculations demonstrate that the formation of morphologies in ABC block copolymers with direct A/C interfaces is possible if the surface tensions between A/B and B/C are large compared to the A/C interface. In our previous work[44] we already mentioned the similarities of this observation to the behavior of homopolymer/copolymer blends, where unfavorable intramolecular repulsive interactions are replaced by less unfavorable interactions between segments of the copolymer and the homopolymer.

The model calculations show that the morphologies which are observed in the SBM and SEBM triblock copolymers can be adequately predicted by simple theoretical arguments. The model correctly predicts that morphological transitions can occur in ABC triblock copolymers by changing the thermodynamic balance even in the strong segregation limit. This is fundamentally different from AB or ABA block copolymers where morphological transitions are limited to the weak segregation limit. "Better" analytical results than those given in the present work would be very painful and at the end it will be unclear whether the results will be closer to experiments and have a better predictive power. The Semenov approximation, which enabled analytical results for the interior and exterior of spherical and cylindrical aggregates requires a strong stretching of chains. In practice chains are rarely strongly stretched in AB block copolymers; i.e. the elastic energy is not many kT per chain. Therefore the stability analysis as given in this paper is instructive owing to its prediction of the cascade of morphological transitions [(ll) → (lc) → (cr) → (ls) or (ll) → (lc) → (ls)].

For a more realistic comparison the calculations could be repeated using more realistic parameters for the Kuhn length and segmental volume of polystyrene, polybutadiene (poly(ethylene-*co*-butene)) and poly(methyl methacrylate). This will considerably change the stability windows of the various morphologies as also has been stated by Birshtein et al.[50] In light of the approximations used in the estimation of the free energy we will not make any further emphasis on such a refinement in the present work. The use of more realistic values of the Kuhn length will also have a profound influence on the predicted dimensions of the microphases. The large differences between the SBM and the SEBM series which cannot be described satisfactorily by the $\gamma^{-1/3}$ dependence may be explained by

the simultaneous variation of the Kuhn length and segmental volume.

So far we restricted the discussion to symmetric triblocks. The opportunities to tailor new mesoscopic microphase morphologies by differences in the degree of incompatibility between the components tremendously increases if asymmetric triblocks are considered. An example of such a very unusual morphology are the helical morphologies which have been observed recently.[57]

Such ABC triblock copolymers are interesting not only because of the new microphase morphologies which can be realized but also because of their unique mechanical properties,[58] and because of their potential as compatibilizers in polymer alloys.[46]

Appendix I. B Spheres at the A/C Lamellar Interface

The geometric parameters used throughout the calculations are given in Figure 6c. A hexagonal packing of B spheres at the A/C interfacial plane is assumed. As for the (ll) and (lc) morphology the discussion will be restricted to the symmetric case i.e. $\phi_A = \phi_C$ ($N_A\nu_A = N_C\nu_C$) and $\gamma_{AB} = \gamma_{BC}$. Despite this we retain the detailed notation to allow the description of nonsymmetric systems at a later stage.

The reduced elementary cell which contains a single sphere has the volume

$$V_{ls}^{r} = \frac{\sqrt{3}}{4} D_{ls}^{2} L_{ls} \tag{I.1}$$

where D_{ls} is the distance between centers of spheres and L_{ls} is the lamellar long period. Under the assumption that the stretching of A and C chains perpendicular and parallel to the direction of the lamella are identical we can write $D_{ls} = L_{ls}/2$.

We define an equivalent sphere of volume

$$V_{ls}^{r} = \frac{\sqrt{3}}{2} D_{ls}^{3} = \frac{4}{3}\pi R_{eq}^{3} \tag{I.2}$$

If Q is the number of chains in the elementary cell and R_B, R_A, and R_C are the radii of the B sphere and A and C shell, the contact areas $\Sigma_{AB,BC}$ are given by

$$\Sigma_{AB} = \Sigma_{BC} = \frac{3}{2}\frac{N_B\nu_B}{R_B} \tag{I.3}$$

and

$$Q = \frac{4\pi R_B^{3}}{3N_B\nu_B} \tag{I.4}$$

For the *AC* interface per chain we can write

$$\Sigma_{AC} = N_B\nu_B \frac{3}{4\pi}\left(\frac{2}{\sqrt{3}}\pi^{2/3} R_{eq}^{2} - \pi R_B^{2}\right)\frac{1}{R_B^{3}} \tag{I.5}$$

Using

$$R_{eq} = R_B \phi_B^{-1/3} \tag{I.6}$$

the surface contribution to the free energy per chain is given by

$$\frac{F_{c(ls)}^{surf}}{kT} = \frac{N_B\nu_B}{R_B}\left(\frac{3}{2}\gamma_{AB} + \frac{3}{2}\gamma_{BC} + \frac{3}{4\pi}\left(\frac{2}{\sqrt{3}}\pi^{2/3}\phi_B^{-2/3} - \pi\right)\gamma_{AC}\right) \tag{I.7}$$

To calculate the elastic contributions of the A and C chains the inhomogeneous stretching of chains in the corona of a sphere is taken into account according to Semenov and Leibler[12,24]

$$\frac{F_{ls,A,C}^{elastic}}{kT} = \frac{1}{2}\frac{R_B^{3}\,\nu_{A,C}}{a_{A,C}^{2} N_B\nu_B}\left(\frac{1}{R_B} + \frac{1}{R_{A,C} + R_B}\right) \tag{I.8}$$

with

$$R_{A,C} = R_B\left[\left(1 + \frac{N_{A,C}\nu_{A,C}}{N_B\nu_B}\right)^{1/3} - 1\right] \tag{I.9}$$

For the elastic potential of the B chains, which again starts at the A/B interface and ends at the B/C interface we follow the same procedure as for the (lc) morphology. In the case of the spheres the average stretching of B chains is given by $L_B = {}^4/_3 R_B$ and thus the elastic potential

$$\frac{F_{ls,B}^{elastic}}{kT} = \frac{8}{3}\frac{R_B^{2}}{N_B\nu_B} \tag{I.10}$$

The prefactor (${}^8/_3$) again can be compared with the value obtained by Semenov for the core of a spherical micelle ($3\pi^2/40$) which is only about ${}^1/_3$ of the value we give.

If the values given by Semenov are used the elastic potential of the B chains is completely underestimated and the (lc) and (ls) morphologies have a lower free energy than the (ll) structure in the whole composition regime.

The total elastic potential is thus given by

$$\frac{F_{c(ls)}^{elastic}}{kT} = \frac{R_B^{2}}{N_B}\left[\frac{1}{2}\frac{\nu_A}{a_A^{2}\nu_B}\left(1 + \left(1 + \frac{\phi_A}{\phi_B}\right)^{-1/3}\right) + \frac{8}{3a_B^{2}} + \frac{1}{2}\frac{\nu_C}{a_C^{2}\nu_B}\left(1 + \left(1 + \frac{\phi_C}{\phi_B}\right)^{-1/3}\right)\right] \tag{I.11}$$

Appendix II: B Rings Surrounding A Cylinders in a C Matrix

The geometric parameters used throughout the calculations are given in Figure 6d. We assume a hexagonal packing of the A cylinders in a C matrix. The cylinder long period is L_{cr}, the distance between the B rings of radius R_B is D_{cr}. The A cylinders have a radius R_A.

The volume of an elementary cell which contains one cylinder of height D_{cr} is

$$V_{cr} = \frac{\sqrt{3}}{2} L_{cr}^{2} D_{cr} \tag{II.1}$$

This volume contains Q chains of volume $N_A\nu_A + N_B\nu_B + N_C\nu_C$. The volume of the B ring is

$$QN_B\nu_B = 2\pi^2 R_A R_B^{2} \tag{II.2}$$

As in the case of the other morphologies we make the assumption that the elastic potential for A and C chains

leaving the B domain is radial, i.e. the extension of A chains parallel and perpendicular to the A cylinder main axis should be very similar. From this it follows approximately that $D_{cr} = 2R_A(f_r)$ ($f_r = 1$); i.e. the distance between the rings is the same as the A cylinder diameter. This is only a crude approximation, which may be acceptable in light of the approximations to come. f_r would be a correction factor to account for an inequality and will not be considered further.

Using this assumption the radius of the A cylinder can be expressed as follows:

$$R_A = R_B\left(\frac{\phi_A}{\phi_B}\pi - \frac{1}{2}\right)^{1/2} \tag{II.3}$$

If the B ring will have a small diameter compared to the A cylinder the contact areas $\Sigma_{AB,BC}$ are identical and can be expressed in terms of R_B

$$\Sigma_{AB} = \Sigma_{BC} = \frac{N_B\nu_B}{R_B} \tag{II.4}$$

The contact area Σ_{AC} can be obtained from the following relation:

$$Q\Sigma_{AC} = 2\pi R_A(D_R - 2R_B) \tag{II.5}$$

Using equation II.3

$$\Sigma_{AC} = \frac{N_B\nu_B}{R_B}\frac{\left(\frac{\phi_A}{\phi_B}\pi - \frac{1}{2}\right)^{1/2} - 1}{2\pi^2} \tag{II.6}$$

The surface free energy per chain thus is given by

$$\frac{F^{surf}_{c(cr)}}{kT} = \frac{N_B\nu_B}{R_B}\left(\gamma_{AB} + \gamma_{BC} + \gamma_{AC}\frac{\left(\frac{\phi_A}{\phi_B}\pi - \frac{1}{2}\right)^{1/2} - 1}{2\pi^2}\right) \tag{II.7}$$

The more difficult task is the description of the elastic contribution to the free energy in the case of the (cr) morphology.

For the B chains the same estimate of L_B can be made as for the (lc) morphology, i.e

$$L_B = \frac{\pi}{2}R_B \tag{II.8}$$

and thus

$$\frac{F^{elastic}_{cr,B}}{kT} = \frac{3}{8}\pi^2\frac{R_B^2}{N_B a_B^2} \tag{II.9}$$

For the A and C chains the situation is much more difficult. The A chains have to fill the A cylinder core. However the equation given by Semenov for the elastic contribution of chains forming a cylinder core will severely overestimate the elastic potential, because the chains emerging from the B rings have also to fill the volume parallel to the A cylinder. This will cause a considerable inhomogeneous stretching which strongly reduces the elastic potential. In other words the A chains act like half of a cylinder corona if the B ring is taken as the reference and acts as the cylinder surface from which the A and C chains emerge. To calculate the exact segment distribution of B segments which would be necessary for the calculation of the elastic free energy is beyond the scope of the present work. In the present approximation we describe the A chains as corona chains emerging from the B cylinder. This will slightly underestimate the elastic potential.

$$F^{elastic}_{cr,A} = \frac{R_B^2}{N_B}\frac{\nu_A}{a_B^2\nu_B}\ln\left(2 + \frac{2}{\pi^{1/2}}\left(\frac{\phi_A}{\phi_B}\pi - \frac{1}{2}\right)^{1/2}\right) \tag{II.10}$$

In the case of the C chains we face similar problems as for the A chains. With respect to the B ring, the C chains are the corona and can be treated in analogy to the (lc) morphology. However due to the curvature of the A cylinder, the gain in configurational space for the C chains with increasing distance from the B rings resembles more closely the situation of a chain in the corona of a sphere. Thus treating the C chains as a cylinder corona will overestimate the elastic potential (upper bound), while the lower bound should be given by the behavior of a corona of a sphere. The larger the radius of the A cylinders the better will be the description of the C chains as the cylinder corona. In the calculations given above we used the following estimate for the elastic contribution of the C chains which will slightly overestimate the elastic potential:

$$F^{elastic}_{cr,C} = \frac{R_B^2}{N_B}\frac{3\nu_C}{2a_C^2\nu_B}\left(1 - \frac{1}{1 + \frac{2}{\pi^{1/2}}qq\left(\left(\frac{\pi}{\phi_B}\right)^{1/2} - qq\right)^{1/2}}\right) \tag{II.11}$$

with

$$qq = \left(\frac{\phi_A}{\phi_B}\pi - \frac{1}{2}\right)^{1/2}$$

As has been mentioned in the main section, the exact formulation will change the size of the stability window of the (cr) morphology, but not the main point of the present paper.

Acknowledgment. This work is supported by the Bundesminister für Forschung und Technologie (BMFT) and by the BASF AG. R.S. acknowledges many discussions with Dr. A. Gottschalk (BASF) and Prof. E. T. Samulski (Chapel Hill, NC). Additional support from the Deutsche Forschungsgemeinschaft (DFG) through SFB 261, project S-14, is gratefully acknowledged. J.B. acknowledges postdoctoral support from the Graduiertenkolleg "Chemie und Physik Supramolekularer Systeme" and from the Sonderforschungsbereich 261.

References and Notes

(1) Molau, G. E. In *Colloidal and Morphological Behaviour of Block Copolymers*; Molau, G. E., Ed.; Plenum Press: New York, 1971.
(2) Riess, G. In *Thermoplastic Elastomers. A Comprehensive Review*; Ledge, N. R., Holden, G., Schroeder, H. E., Eds.; Hanser: Munich, 1987; Chapter 12.2, p 325.
(3) Meier, D. J., Ed. *Block Copolymers: Science and Technology*; Gordon & Breach Science Publisher: Tokyo, 1983.
(4) Kinning, D. D.; Thomas, E. L.; Alward, D. B.; Fetters, L. J.; Handlin, D. L. *Macromolecules* **1986**, *19*, 1288, 2197.
(5) Hasegawa, H.; Tanaka, H.; Yamasaki, K.; Hashimoto, T. *Macromolecules* **1987**, *20*, 1651.
(6) Meier, D. J. *J. Polym. Sci.* **1969**, *C26*, 81.
(7) Helfand, E.; Sapse, A. M. *J. Chem. Phys.* **1975**, *62*, 1327.
(8) Helfand, E.; Wasserman, Z. R. *Macromolecules* **1976**, *9*, 879.
(9) Helfand, E.; Wasserman, Z. R. *Macromolecules* **1978**, *11*, 960.
(10) Alexander, S. *J. Phys. (Paris)* **1977**, *38*, 983.
(11) de Gennes, P. G. *Macromolecules* **1980**, *13*, 1069.

(12) Semenov, A. N. *Sov. Phys. JETP* **1985**, *61*, 733.
(13) Förster, S.; Khandpur, A.; Schulz, M. F.; Bates, F. S. *Bull. Am. Phys. Soc.* **1993**, *38*, 605.
(14) Semenov, A. N. *Macromolecules* **1994**, *27*, 3103.
(15) Hajduk, D. A.; Harper, P. E.; Gruner, S. M.; Honeker, C. C.; Kim, G.; Thomas, E. L.; Fetters, L. J. *Macromolecules* **1994**, *27*, 4063.
(16) Matsen, M. W.; Schick, M. *Phys. Rev. Lett.* **1994**, *72*, 2660.
(17) Bates, F. S.; Rosedale, J. H.; Fredrickson, G. H.; Glinka, C. J. *Phys. Rev. Lett.* **1988**, *61*, 2229.
(18) Bates, F. S.; Rosedale, J. H.; Frederickson, G. H. *J. Chem. Phys.* **1990**, *92*, 6255.
(19) Holzer, B.; Lehmann, A.; Strobl, G.; Stühn, B.; Kowalski, M. *Polymer* **1991**, *32*, 1935.
(20) Stühn, B.; Mutter, R.; Albrecht, T. *Europhys. Lett.* **1991**, *32*, 1935.
(21) Leibler, L. *Macromolecules* **1980**, *13*, 1602.
(22) Frederickson, G. H.; Helfand, E. *J. Chem. Phys.* **1987**, *87*, 697.
(23) Leibler, L. *Macromolecules* **1982**, *15*, 1283.
(24) Leibler, L. *Makromol. Chem., Makromol. Symp.* **1988**, *16*, 1.
(25) Hong, K. M.; Noolandi, J. *Macromolecules* **1984**, *17*, 1531.
(26) Noolandi, J.; Hong, K. M. *Macromolecules* **1982**, *15*, 482.
(27) Budkowski, A.; Steiner, U.; Klein, J.; Fetters, L. J. *Europhys. Lett.* **1992**, *18*, 499.
(28) Brown, H. R.; Char, K.; Deline, V. R. *Macromolecules* **1990**, *23*, 3383.
(29) Shull, K. R.; Kramer, E. J.; Hadziioannou, G.; Tang, W. *Macromolecules* **1990**, *23*, 4780.
(30) Budkowski, A.; Klein, J.; Steiner, U.; Fetters, L. J. *Macromolecules* **1993**, *26*, 2470.
(31) Binder, K. *Adv. Polym. Sci.* **1994**, *112*, 182.
(32) Zielinski, J. M.; Spontak, R. J. *Macromolecules* **1992**, *25*, 663. Spontak, R. J.; Zielinski, J. M.; Lipscomb, G. G. *Macromolecules* **1992**, *25*, 6670. Smith, S. D.; Spontak, R. J.; Satkowski, M. M.; Shraf, A.; Lin, J. S. *Phys. Rev.* **1993**, *B47*, 14555.
(33) Gido, S. P.; Gunther, J.; Thomas, E. L.; Hoffman, D. *Macromolecules* **1993**, *26*, 4506.
(34) Koizumi, S.; Hasegawa, H.; Hashimoto, T. *Macromolecules* **1994**, *27*, 4371. Hashimoto, T.; Yamasaki, K.; Koizumi, S.; Hasegawa, H. *Macromolecules* **1993**, *26*, 2895. Hashimoto, T.; Yamasaki, K.; Koizumi, S.; Hasegawa, H. *Macromolecules* **1994**, *27*, 1562.
(35) Riess, G.; Schlienger, M.; Marti, S. *J. Macromol. Sci., Polym. Phys. Ed.* **1980**, *17* (2), 355.
(36) Arai, K.; Kotaka, T.; Kitano, Y.; Yoshimura, K. *Macromolecules* **1980**, *13*, 1670.
(37) Kudose, I.; Kotaka, T. *Macromolecules* **1984**, *17*, 2325.
(38) Matsushita, Y.; Choshi, H.; Fujimoto, T.; Nagasawa, M. *Macromolecules* **1980**, *13*, 1053.
(39) Shibayama, M.; Hasegawa, H.; Hashimoto, T.; Kawai, H. *Macromolecules* **1982**, *15*, 274.
(40) Mogi, Y.; Kotsui, H.; Kaneko, Y.; Mori, K.; Matsushita, Y.; Noda, I. *Macromolecules* **1992**, *25*, 5408.
(41) Mogi, Y.; Mori, K.; Matsushita, Y.; Noda, I. *Macromolecules* **1992**, *25*, 5412.
(42) Mogi, Y.; Mori, K.; Kotsuji, H.; Matsushita Y.; Noda, I.; Han, C. *Macromolecules* **1993**, *26*, 5169.
(43) Gido, S. P.; Schwark, D. W.; Thomas, E. L.; Goncalves, M. C. *Macromolecules* **1993**, *26*, 2636.
(44) Auschra, C.; Stadler, R. *Macromolecules* **1993**, *26*, 2171.
(45) Auschra, C.; Beckmann, J.; Stadler, R. *Macromol. Rapid Commun.* **1994**, *15*, 67.
(46) Auschra, C.; Stadler, R. *Macromolecules* **1993**, *26*, 6364.
(47) Adjari, A.; Leibler, L. *Macromolecules* **1991**, *24*, 1991.
(48) Nakazawa, H.; Ohta, T. *Macromolecules* **1993**, *26*, 5503.
(49) Kane, L.; Spontak, R. J. *Macromolecules* **1994**, *27*, 663.
(50) Birshtein, T. M. Personal communication. Lyatskava, Y. V.; Birshtein, T. M. *Polymer*, in press.
(51) Auschra, C.; Stadler, R. *Polym. Bull.* **1993**, *30*, 257.
(52) Auschra, C.; Stadler, R. *Polym. Bull.* **1993**, *30*, 305.
(53) Anastasiadis, S. H.; Russel, T. P.; Satija, S. K.; Majkrzak, C. F. *J. Chem. Phys.* **1990**, *92*, 5677. Semenov, A. N. *Macromolecules* **1993**, *26*, 6617.
(54) Auschra, C. Doctoral Dissertation, Johannes Gutenburg Universität, Mainz, 1992.
(55) R.S. is indebted to Prof. M. Möller (Ulm), Prof. J. DeSimone, and Prof. E. T. Samulski (both UNC, Chapel Hill, NC) who independently indicated the existence of similar micrographs in ref 34.
(56) Hashimoto, T.; Sakurai, S.; Momii, T.; Taie, K.; Shibayama, M.; Nomura, S.; Hashimoto, T. *Macromolecules* **1993**, *26*, 485.
(57) Krappe, U.; Stadler, R.; Voigt-Martin, I. G. Submitted to *Macromolecules*.
(58) Auschra, C.; Beckmann, J.; Krappe, U.; Stadler, R. To be published.

MA941303E